FINAL REPORT

Taiwan – US AFOSR Nanoscience Initiative (AOARD-06-4067)

Covalent Percolation and Gold Templating of Carbon NanoTubes Network in Polymer Nanocomposites for Novel Mechanical, Electrical, and Optical Properties

Principal Investigator
Arnold C.-M. Yang

acyang@mse.nthu.edu.tw

Department of Materials Science and Engineering
National Tsing Hua University

101, Kuang Fu Road, Section 2, Hsinchu City, Taiwan
Phone: +886-3-572-0792, FAX: +886-3-572-2366

Report Documentation Page

Form Approved
OMB No. 0704-0188

1. REPORT DATE	2. REPORT TYPE	3. DATES COVERED
26 MAR 2008	**Final**	**01-07-2006 to 30-06-2007**

4. TITLE AND SUBTITLE
Covalent Percolation and Gold Templating of Carbon NanoTubes Network in Polymer Nanocomposites for Novel Mechanical, Electrical, and Optical Properties

5a. CONTRACT NUMBER
FA48690610093

5b. GRANT NUMBER

5c. PROGRAM ELEMENT NUMBER

6. AUTHOR(S)
Arnold Chang-Mou Yang

5d. PROJECT NUMBER

5e. TASK NUMBER

5f. WORK UNIT NUMBER

7. PERFORMING ORGANIZATION NAME(S) AND ADDRESS(ES)
National Tsing Hua University,101, Kuang Fu Rd, Sec 2,Hsinchu,Taiwan,NA,NA

8. PERFORMING ORGANIZATION REPORT NUMBER
N/A

9. SPONSORING/MONITORING AGENCY NAME(S) AND ADDRESS(ES)
AOARD, UNIT 45002, APO, AP, 96337-5002

10. SPONSOR/MONITOR'S ACRONYM(S)
AOARD

11. SPONSOR/MONITOR'S REPORT NUMBER(S)
AOARD-064067

12. DISTRIBUTION/AVAILABILITY STATEMENT
Approved for public release; distribution unlimited

13. SUPPLEMENTARY NOTES

14. ABSTRACT
The interactions between individual polymer chains with embedded carbon nanotubes (CNTs) in nanocomposites were investigated by using two model polymer systems, polystyrene and poly(phenylene oxide) representing respectively the ductile and brittle polymers, with surface-grafted multiwalled CNTs.

15. SUBJECT TERMS

16. SECURITY CLASSIFICATION OF:			17. LIMITATION OF ABSTRACT	18. NUMBER OF PAGES	19a. NAME OF RESPONSIBLE PERSON
a. REPORT	b. ABSTRACT	c. THIS PAGE			
unclassified	**unclassified**	**unclassified**	**Same as Report (SAR)**	**82**	

Chapter 1

Interactions of polymer chains with multiwalled carbon nanotubes during microscopic plastic flow in glassy nanocomposites

Abstract

The interactions between individual polymer chains with the embedded carbon nanotubes (CNTs) in the nanocomposites were investigated by using two model polymer systems, polystyrene (PS) and poly(phenylene oxide) (PPO) representing respectively the ductile and brittle polymers, with surface-grafted multiwalled CNTs. Although significant mechanical reinforcement was both clearly observed, drastically different interactions that stemmed from the fundamental chain behavior of the entangled chains were noted during the micro-plastic flow processes of the nanocomposites. It was found that, by a local stress analysis based on the atomic force microscopic topography, strain hardening of the entanglement network determines not only the mode of chain deformation that leads to either brittle or ductile failure but also how the sliding chains interact with individual nanotubes. The results bear important implications on our understanding toward the fundamental behavior of entangled macromolecules in the glassy state.

1-1 Introduction

The nanocomposites based on well dispersed carbon nanotubes (CNTs) embedded in carefully selected polymer matrices have attracted increasingly attentions due to their great potentials for innovated mechanical, electrical, thermal, and opto-electronic properties. The outstanding advantageous properties of CNTs, such as the exceedingly high Young's modulus [1-2] and conductivities, large flexibility limits and fracture strains [3], and simply being tiny tubules of high aspect ratios, have made CNT an ideal filler for most polymers. In this context, the interactions between the embedded CNTs and the surrounding polymer chains not only are very interesting in the light of unveiling the fundamental chain behavior of

the entangled macromolecules. They but also are of vital importance due to requirement of effective reinforcement down to the nanometer scales for successful modifications of the physical properties.

Previous works on CNTs as fillers in polymers have been focused primarily on the low-strain elastic behavior and cracking properties [4-13]. Little attentions had been paid to the more important plastic flows regime that constitutes the major part of the mechanical performance before fracture. The elastic modulus and breaking stress in polystyrene (PS) were shown by Qian *et al*. [7,14] to increase significantly by the addition of CNTs, pointing to the significant role of load transfer of CNTs. Watts *et al*. [15] also identified the pull-out mechanism of CNTs in bridging a crack, which effectively retarded the cracking process in the CNTs-PS thin films. Apparently, such observations of the effects of CNTs on stress transfer mechanisms or failure processes strongly depend on the state of CNT dispersion and their interactions with the polymer chains. Moreover, given the above-mentioned reinforcement effects, it is hard to comprehend why the best reinforcement results in CNT-polymer composites were observed only when a small volume fraction of CNTs [8,11,16-18] was added; for higher CNTs loadings (> 5%), the mechanical properties generally fell off [9,19]. This indicates the necessity of more in-depth investigation of the interactions between CNTs and polymer chains over a wider range of deformation including both the elastic and plastic behavior.

It is well known that glassy polymers develop microscopic deformation zones before fracture. The stress-induced local plastic flow that gives rise to the formation of microscopic deformation zones of crazes [29-32] or shear deformation zones (SDZs) triggers extraordinarily large plastic strains (~ 200 – 300%) and is the main molecular mechanism for yielding in most glassy polymers. The occurrence of crazes or SDZs depends on the entanglement density ν_e of the polymer matrix defined as $\nu_e = \ell_e/d$ where ℓ_e is the contour chain length between entanglement points and d the direct distance between them [Kramer, our papers]. When $\nu_e > \nu_e^c$ (tight networks), shear deformation zones prevails and crazes dominate the regime of $\nu_e < \nu_e^c$ (loose networks) with $\nu_e^c \sim 6 \times 10^{25}/m^3$ [29]. In

addition, crazing and shear yielding represent respectively the precursor of brittle and ductile fracture of glassy polymers. They are both produced by micronecking induced during the plastic flow but the microstructures are quite different to each other with the crazes being constructed by interconnected fibrils embedded in a void while SDZs the smoothly thinned solid regions (Fig. 1) [20-22]. The effect of CNTs on chain movements during deformation thus can be best revealed in the CNT interactions with the respective microdeformation zones of crazes and SDZs.

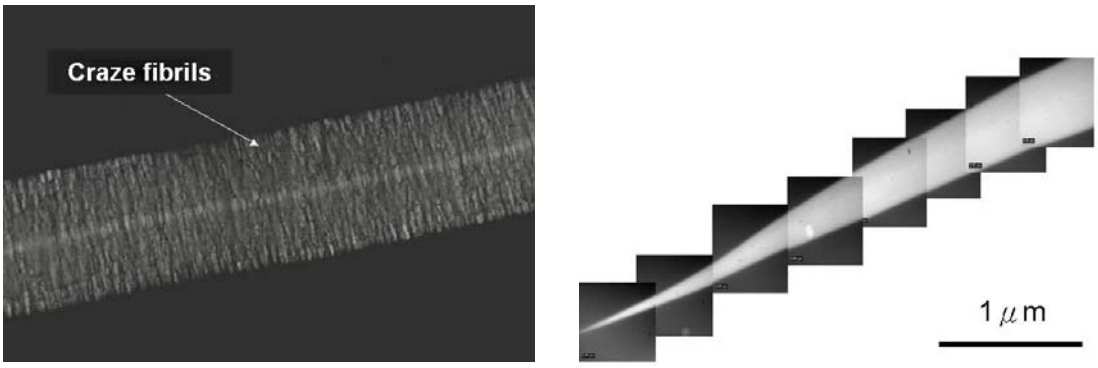

(a) (b)

Figure 1. TEM micrographs of the craze (left) and shear deformation zone (right).

Previously, the role of MWCNTs during crazing in brittle polymer was explored by investigating the nanocomposite films of PS blended with surface-grafted MWCNTs [21-22]. The micro-necking characteristics induced by crazing were not modified by the presence of MWCNTs but the process was strongly suppressed. As a result, only short and narrow crazes were formed. Moreover, the MWCNTs were generally not found inside the micro-deformation zones but, instead, piled up at the craze boundaries. The delocalization of strains forced by interactions with MWCNTs substantially enhanced the toughness of PS films that showed no cracks even at strains greater than 20 % with only 1.5 wt.% MWCNT loading. In this study, more thorough investigation of the interactions between MWCNTs and polymer chains was undertaken by further focusing the MWCNTs reinforcement in PS and comparing that in SDZ-forming poly(phenylene oxide) (PPO). As a result,

interesting and revealing information was emerging that should shed light on the fundamental micro-mechanical behavior of the important CNTs-polymer nanocomposites.

1-2 Experimental section

Monodisperse PS of molecular weight (*M*w) = 2,000,000 g/mol. (Pressure Chemical Co., U.S.A.) was used. The polymer PPO (Aldrich Chemical Co.) with a molecular weight of 244,000 g/mol. Was used as-received. The MWCNTs (DESUN Nano Co., Taiwan) used in this study were found to have an average outer diameter around 10-35 nm and a length of 10-30μm.

Methods for fabricating of PS-g-MWCNTs have been reported previously [21-22]. Briefly, the PS surface grafting on the MWCNTs was carried out in three consecutive steps. First, the nanotubes were surface-treated by anchoring carboxylic acid groups onto the tube external surfaces (MWCNTs–COOH) and the total percentage of acidic sites in the full length MWCNT is about 3.5wt.% (determinate by the acid-base titration). Then, the carboxylic acid groups in MWCNTs–COOH were esterified by further reactions with 4-vinylbenzyl chloride to produce –COOR groups grafting on the tube surfaces (MWNTs–COOR). Finally, the grafted groups on the tube surfaces were put into the polymerization reaction, initiated with 2,2-azobisisobutyronitrile (AIBN), with styrene monomers. The chain lengths of the grafted PS on MWNT (PS-MWCNTs) was showed the Mw = 60000 g/mol (polydisperity=2.1) from the gel permeation chromatography (GPC) data by the defunctionalization method [23], and the grafted amount of PS on MWCNTs is about 60 wt.% (calculated from TGA data) and average length of PS-g-MWCNTs is 1-3 μm.

The PS-grafted MWCNTs were mixed, by approximately 2 wt. % in weight, with the PS (or PPO) in toluene solution. The MWCNTs/PS (or MWCNTs/PPO) films were spun cast from the solution, and the film thickness was controlled to be around 0.5μm. The MWCNTs/Polymer films were floated off the substrate on distilled water and bonded onto supporting copper grids and the MWCNTs/PPO films needs to aging at 120□ for 1 hour before testing. After following the proper bonding procedure, the specimen was mounted in a strain jig and stretched under

an optical microscope to observe the growth of local deformation zones (crazes or SDZs) [21,24-28]. The stretched MWCNT/Polymer films were then examined under an AFM (Digital Instrumental, Nanoscope IIIa) to investigate the topographic information. The AFM topographic data were used to calculate the local nanomechanical information in the local deformation zones [27-28]. A transmission electron microscopy (TEM, JEOL JEM-2010) was used to obtain images of the microstructures of the MWCNTs/polymer films. Craze widening was monitored by a video camera that was attached to an optical microscope. The speed of craze widening was determined from the collected images of the growing crazes.

1-3 Results and Discussions

Craze morphology modified by MWCNTs

Crazes initiated at approximation 1% strain (ε) in the pristine PS films and they were generally straight, widening steadily as the strain increased, and the maximum width of creases could reach approximately 18 μm (Figure 2a). Local fibril breakdowns within the crazes started at approximately ε = 8%. Craze surface topography determined from AFM revealed that craze depth d determined from AFM, increased almost linearly with craze width w when $w < w_c$, Figure 3a, where w_c is the critical craze width that is a function of film thickness (for 0.5 μm thick PS film, $w_c \sim 2.5$ μm) and representing the start of the microneck propagation [21]. For $w > w_c$, craze depth became constant with w, indicating steady-state drawing of the crazing plastic flow. In contrast to the pristine films, the MWCNTs/PS (MWCNTs content 2 wt.%) films shown a quite different mechanical behavior in that the crazes remained short and narrow (mostly less than 2 μm wide) and no micro-cracking was observed even at large strains greater than 20% (Figure 2b). It strongly indicated that by delocalization of the plastic flow the MWCNT networks embedded in the PS film had dramatically increased the toughness of the glass polymer. Furthermore, although the curve of depth versus width followed closely that of the prinstine PS, the craze width in MWCNTs/PS films never reached w_c. The observations at this level were consistent with that reported before [21] which describes in more detailed the micro-deformation behavior and thus will not

reiterate further here.

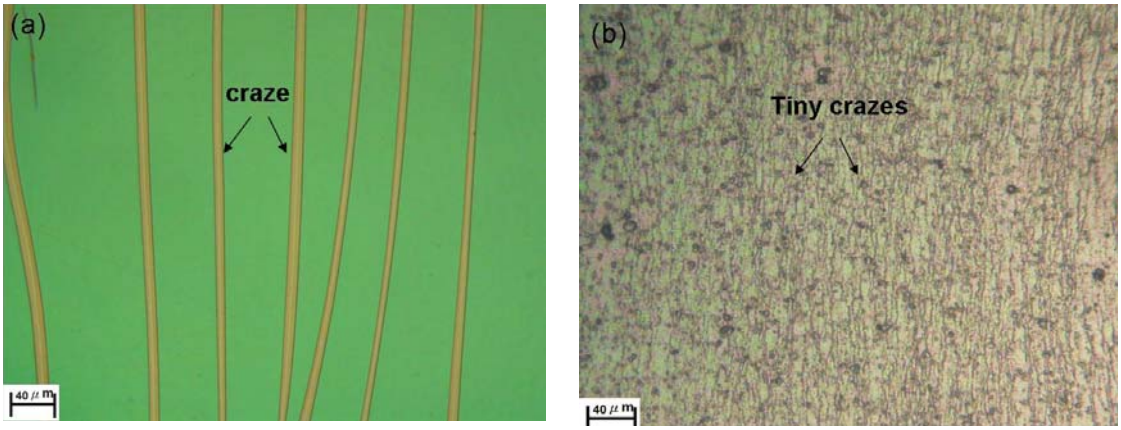

(a) (b)

Figure 2. Optical micrograph of stretched (a) pristine PS films and (b) MWCNTs/PS composite film (weight fraction of MWNT is 2 wt%).

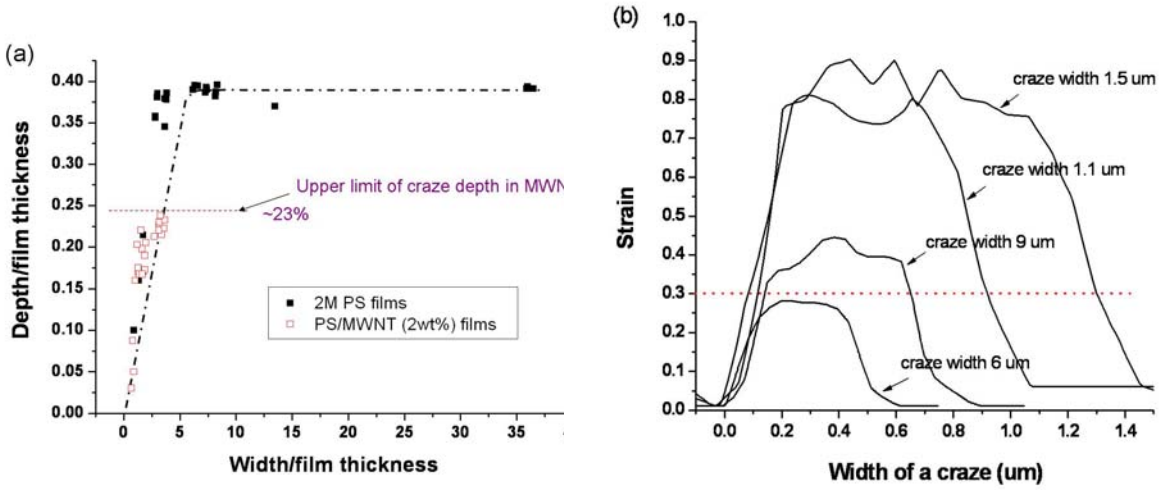

Figure 3. Local strain distribution across the craze width.

The strain distribution within the craze was determined by calculations from the AFM craze topography under the plastic deformation assumption [27,huchingson, desocise]. For either the pristine PS or the nanocomposite film of MWCNTs/PS, the strain, as expected, concentrated within the craze, forming a plateau in the craze center (ref. 21, Figure 3b). The plateau strain ε_p increased with craze width w

but tended to saturate for wider crazes (w > 1 μm) Note that the plateau strain within the craze is just below 30%, the reported elastic limit of carbon nanotubes [3], for crazes thinner than 0.6 micron in width.

Figure 4a shows a TEM micrograph of a craze tip propagating into a region of visibly populated MWCNTs. The presence of the MWCNTs, as it clearly shows, has no effect on the growth the craze in that the craze tip penetrates right through the MWCNTs. Note that the maximum strain within the craze (the plateau strain) is below the elastic limit of MWCNTs in crazes thinner than ~ 0.6 μm, it would thus be of no surprise that MWCNTs could be easily survived incorporating into narrow crazes without inflicting breakage of the MWCNTs or incurring substantial modification of the craze drawing process. In contrast, thorough investigation under TEM has revealed that wider crazes (Figures 4b and c) rarely showed MWCNTs inside the crazes. Most of the time the MWCNTs were either fractured, leaving broken ends at boundaries of the wider crazes (Figure 4c), or simply staying outside. Incorporating intact MWCNTs into crazes occurred only rarely when small isolated “pockets” in the film were first surrounded by crazed regions and then “swallowed” unfibrillated into and forming islands inside the crazes; the MWCNTs were then exposed within the crazes when the small islands later underwent fibrillation. As strongly hinted by Figure 3, the large strains within the interior of the crazes with w > ~ 0.6 μm has forced the competition between nanotube breakage and craze drawing of MWCNTs to occur. Apparently it seems impossible for the PS chain network to pull the MWCNTs into the micro-deformation zones. Hence, they broke or remained excluded from the crazed region. The exclusion of MWCNTs, as will be illustrated in the following, has caused an increased difficulty of chain fibrillation at the later stages.

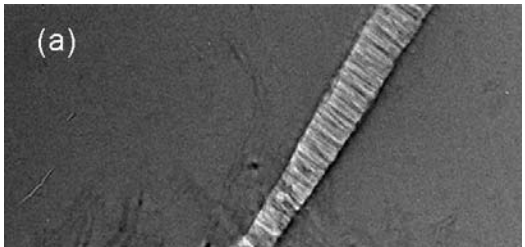

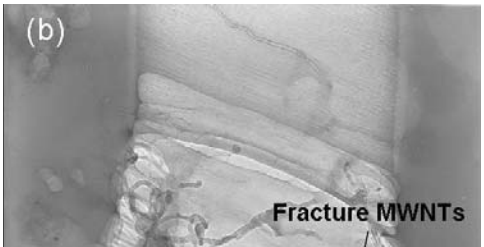

(a) **(b)**

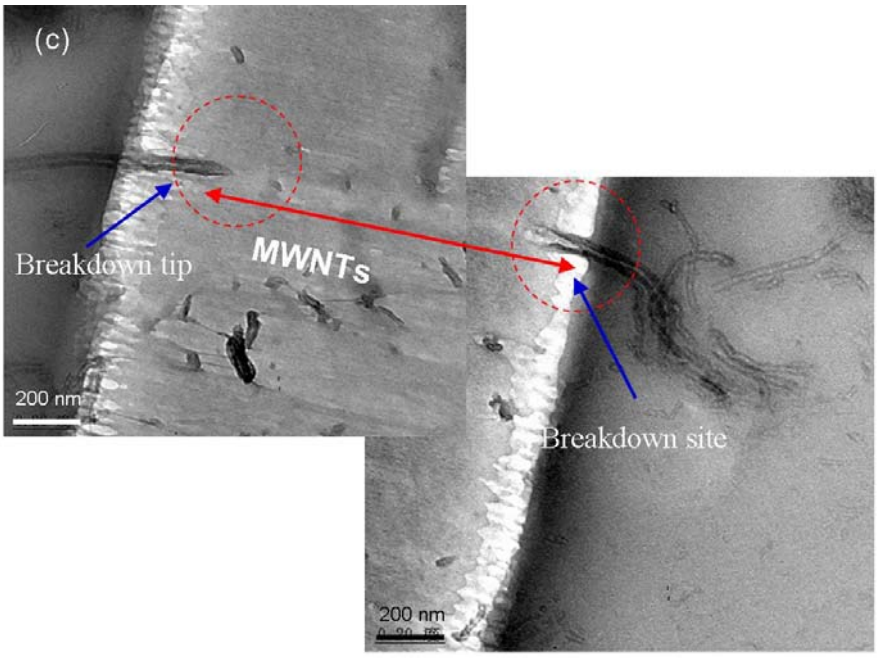

(c)

Figure 4. TEM micrographs of (a)craze tip, (b) wider craze in MWCNT/PS films (weight fraction of MWCNT is 2 wt%), and (c) fracture of nanotubes in MWCNT/PS films (weight fraction of MWCNT is 2 wt%).

Exclusion of MWCNTs from craze drawing

The exclusion of MWCNTs from the crazing process was examined following the steps described in ref. 21 by mildly etching the crazed samples of MWCNTs/PS by oxygen plasma at 60 W. Consistent with the previous discovery, protrusions due to the pileup of the slow-etching MWCNTs were observed bulging along the banks on both sides of the crazes as revealed from AFM topographic analysis of the etched surface. The width of the protrusion was found to increase with etching time and then leveled off (inset of Figure 5a) and the plateau width (typically taking ~ 9 min. etching time) was plotted against the width of craze width. As clearly seen in Figures 5a, the width of the MWCNT ridges increased as craze width increased. This is consistent with the notion inspired by the TEM observations (Figure 5b) that MWCNTs were excluded from craze fibrillation in PS films, and thus the wider crazes, the more pileup of the MWCNTs at the boundaries of the crazes. The height of the MWCNT ridges ranged from 60 to 120 nm, with the ridge width varying from 210 to 320 nm, at various craze widths.

Base on these data, we attempted to calculate the local MWCNTs density at the craze boundaries since MWCNTs would certainly modify or even change the craze drawing if they piled up at the gateways of micronecking. Here, we assumed all of MWCNTs were excluded from the crazes during the crazing process and piled up at protruding ridges regions. Thus, the local concentration of the piled-up MWCNTs at craze boundaries (C_{pu}) will depends on the original concentration of MWCNTs (C_0) in the nanocomposite film, the widths of craze and protruding ridges, and the draw ratio of the deformation zones. It can be written as

$$C_{pu} = C_0 (1 + W_c\, dz\, D / 2\, W_d\, \delta) \qquad (1)$$

Where Wc is the width of craze, dz is the thickness of craze, D is the density of craze (D= 0.8 g/cm^3), Wd is the width of pileup MWCNTs at the boundaries, and δ is film thickness of MWNTs/PS films. Figure 5c depicts that the local MWCNTs concentrations at the pileup calculated from the width of the MWCNT ridges increases with craze width. The slope obviously increases with the concentration of MWCNTs in the film. The increase of MWCNT concentration in fact is significant and fast. For example, for the film with 2 wt% of MWCNTs, the local MWCNT

concentration at the craze boundaries goes up to 8 wt.% for a 2μm wide craze. It clearly indicated that when a craze grows wider, the PS chains to be drawn from outside the deformation zone need to pass through a denser network of MWCNTs at the craze boundaries. Thus, a greater drawing stress is required for the PS chains to overcome the resistance arising from flowing through the MWCNTs network, and thus craze widening becomes more and more difficult.

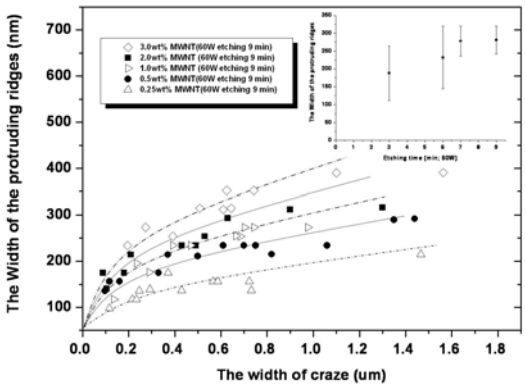

(a)

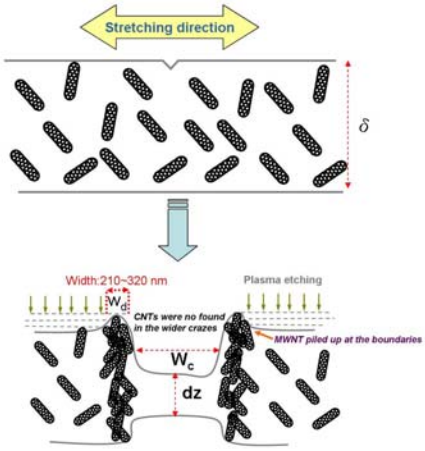

(b)

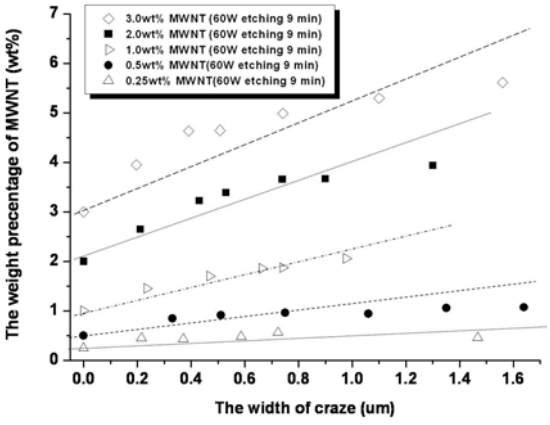

(c)

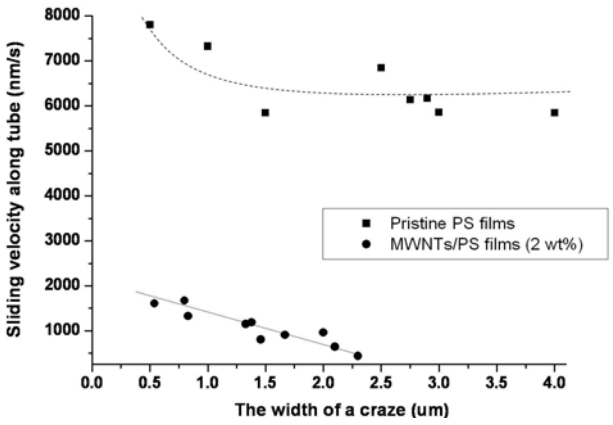

(d)

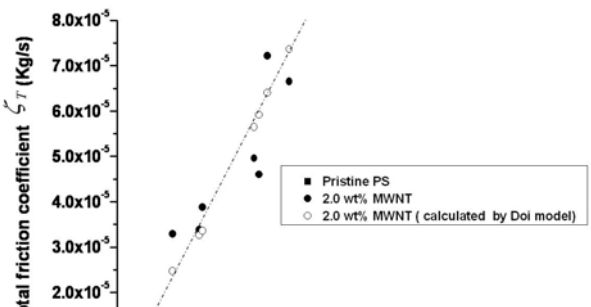

(e)

Figure 5. (a).The width of the MWCNT piled up at the craze boundaries versus craze width, (b) a schematic of the MWCNT piled up at the craze boundaries, (c) the weight percentage of MWCNT protruding vs width of craze in MWNT/PS films, (d) the sliding velocity of a PS chain vs width of craze in pristine PS and MWCNT/PS films, (e) the total friction coefficient of a PS chain vs width of craze in pristine PS and MWCNT/PS films. (inset) The width of the MWCNT piled up at the craze boundaries exposed at 60W oxygen plasma with different etching time.

Fibrillation modified by MWCNTs

For further quantitative analysis on the restricted widening of crazes, the chain friction coefficient during craze widening was calculated by using a Rouse chain model. The drawing of a polymer chain into the craze is simulated by a scenario where the polymer chain is under a constant force (f) that pulls the chain with a constant velocity (v) along the "topological tube" defined by neighboring chain entanglements. The force and velocity are related by the total frictional coefficient ζ_R of the whole Rouse chain, as

$$f = v\,\zeta_R \qquad (2)$$

The force that is pulling the chain into the craze can be determined from the drawing stress s during crazing and the cross-sectional area of the chain within the tube A_{tube},

$$f = \sigma A_{tube} \qquad (3)$$

The area of the confining tube (A_{tube}) is approximately 0.688 nm^2 for a single PS chain in the tube where in average a total of 22 chains share the tube space [38].

For pristine PS films, the drawn stress (σ) during the crazing process can be calculated from AFM topography data [27-28] and at steady state drawing ($w > w_c$) it was approximately σ = 94 MPa. Thus the drawing force was calculated by Eq. (2) to be f = 0.065 nN. On the other hand, the velocity of polymer chain sliding along the tube was calculated from the craze widening velocity at the steady state, multiplied by a correction factor of $N^{1/2}$, where N is the number of Kuhn monomer in the tube, to take into account the fact that the chain conformation follows that of a random coil [39]. The craze widening velocity was measured at the steady state by video camera recording of growth of the craze, approximately to be 140 nm/s. For PS, taking the Kuhn monomer molar mass to be 720 g the number of Kuhn monomer N is approximately 2800 for chains of molar mass of 2M g. Thus the chain sliding velocity along the tube (v) is v ~ 7380 nm/s, as shown in Figure 5d. In the pristine PS film, the chain sliding velocity along the tube was slightly decrease with the craze winding, it maybe due to the strain hardening effect at surface drawing process. However, when craze width reached to w_c the chain sliding velocity along the tube was tend to a constant. Base on above results, that gives the friction coefficient of pristine PS ($\zeta_{PS\text{-}PS}$) to be $\zeta_{PS\text{-}PS}$ = 1.13×10^{-5} k g/s. On the other hand, the chain sliding velocity along the tube in the MWCNT/PS composite films was shows decrease almost linearly with craze width.

In the MWCNT/PS composite films, MWCNT pileup at the craze boundaries would undoubtedly increase the frictional force as polymer chains were pulled into the craze. For the sake of simplicity, several approximations were made here. Firstly, the total friction coefficient (ζ_T) was assumed to be linearly comprised of contributions from frictions with neighboring chains as well as that arising from the MWCNT network. The friction coefficient (ζ_T) at craze boundaries can thus be obtained from the Eqs. (2-3) and the data in Figure 5c, 5d. Figure 5e shows the friction coefficient of a PS chain drawn into a craze, estimated using the approximate method just described, as a function of craze width for sample of 2wt% MWCNTs. The results strongly indicated the pileup of MWCNTs at craze

boundaries increased chain friction, thus restricting widening of crazes and forcing new crazes initiation in the non-pileup regions to absorb the applied strain. As a result, the crazes were all short and narrow. Since craze fibril stability decreases exponentially with fibril length (craze width) [31, 40], smaller crazes survive higher strain and do not break down easily. Therefore the toughness increases dramatically.

Base on these results we know that the friction coefficient of a PS chain drawn into a craze was strongly depending on the local MWCNTs concentration (local viscosity). The rheological property of CNTs/polymer nanocomposites has been studied [41] by taking an analogy to that of the rigid-rod polymer in a solution [42] owing to CNT's high aspect ratio. The steady shear flow viscosity η of a semidilute solution of rigid-rod particles depends on the concentration (the number of MWNTs per volume) (c), length (L), and diameter (D) of the particles, as shown below:

$$\eta = \eta_S (1 + \frac{\pi}{30\beta} \frac{(cL^3)^3}{\ln(\frac{L}{D})}) \quad (4)$$

where β is a numerical factor ($\beta = 1.32 \times 10^3$). Moreover, the chain conformation in the MWCNTs/PS systems is assumed to be approximately the same as that in pristine PS such that the length and molar mass of the Kuhn monomer remain unchanged. Since the friction coefficient ζ is proportional to the viscosity, thus taking η_s to be $\zeta_{PS\text{-}PS}$ and η to be ζ_T, the latter was calculated from the average length and diameter of the MWCNTs. Steady shear flow viscosity predicts the relationship between the friction coefficient of a PS chain drawn into a craze and craze width for MWCNTs/PS films was also shown in Figure 5e. For the best fitting result, the length (L) of MWNTs is 1.4 μm and diameter (D) to be 35 nm.

Embrittlement due to MWCNTs

However, embrittlement follows as the MWCNTs content increases to above 3 wt.%. (More data) The embrittlement is due to the increase of not only the drawing stress for craze widening, but also the craze initiation stress. Eventually, few crazes can be drawn to absorb the deformation, and cracking becomes the preferred option (Figure 6a and 6b).

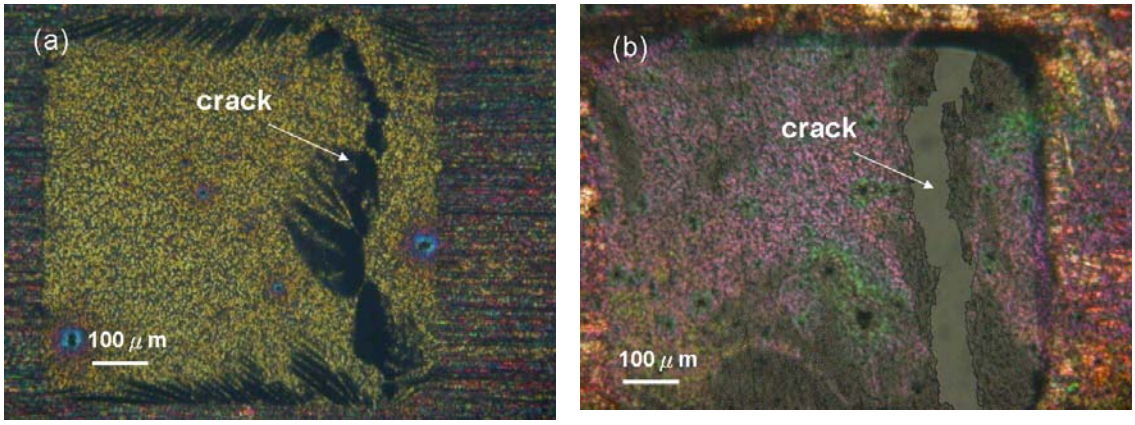

Figure 6. Optical micrograph of stretched MWCNT/PS films at high MWCNTs content (a) 3wt% and (b) 5 wt%.

Interactions between of MWCNTs and SDZs

Shear deformation zone (SDZs) are commonly observed in ductile polymers, such as PPO, and they show quite different microstructure to that of crazes. The material within a SDZ is not fibrillated as are the craze fibrils, rather it is a uniformly thinned polymer sheet drown by the necking stress to a almost uniform extension ratio. To localize the strain, the pristine PPO film was aged at 120 □ for 1 hour before being stretched to grow SDZs. The SDZs nucleated at approximately ε = 2%, to be straight and long, with sharp boundaries as viewed under an optical microscope. They widened steadily as strain increased and eventually broke down to form cracks as ε > 13% (Figure 7a). (The zones could be drawn to a width as far as 40 micron (> 8 μm) before voids were initiated.) Under an AFM, the depth *d* of the SDZs followed a micronecking characteristic in that *d* increased linearly with w until w = w_c and thereafter leveled off to a constant depression (Figure 8a). The smooth surface of the SDZs, however, showed wavy fine striations lines under TEM that were perpendicular to the stretching direction. These striations may have revealed fine features arising from deformation of the PPO entanglement chains network.

The straight and fat SDZs observed in the neat PPO films underwent drastic changes when small amount of MWCNTs were added into the polymer matrix. The

SDZs became short and narrow (less than 8 μm wide), more numerous, and the film remained intact without forming micro cracks even at strains greater than 16% (Figure 7b). This effect due to MWCNTs is quite similar to that observed in MWCNTs/PS systems where strain delocalization reinforced the brittle polymer. (Why?) These SDZs, however, illustrated a very different mode of interactions with the embedded MWCNTs in that the MWCNTs were drawn into the SDZs, as revealed by TEM microscopy. Figure 7c and 7d shows the MWCNTs drawn into narrow (Figure 7c) and wide (Figure 7d) SDZs. The MWCNTs of smaller diameter (ca. <20 nm) were clearly straightened along the drawing direction of the plastic flow. For these MWCNTs of greater diameter, alignment of the CNTs appeared to be more difficult and local debonding between the MWCNTs and the polymer matrix was frequently observed (Figures 7c and d). Consistent with the TEM observation, the etched SDZ topography did not show any pileup of MWCNTs at the edges (Figure 8b) under AFM. It is clear that the MWCNTs embedded in the PPO matrix can be drawn into the SDZs along with the stress-induced plastic flow of the glassy polymer.

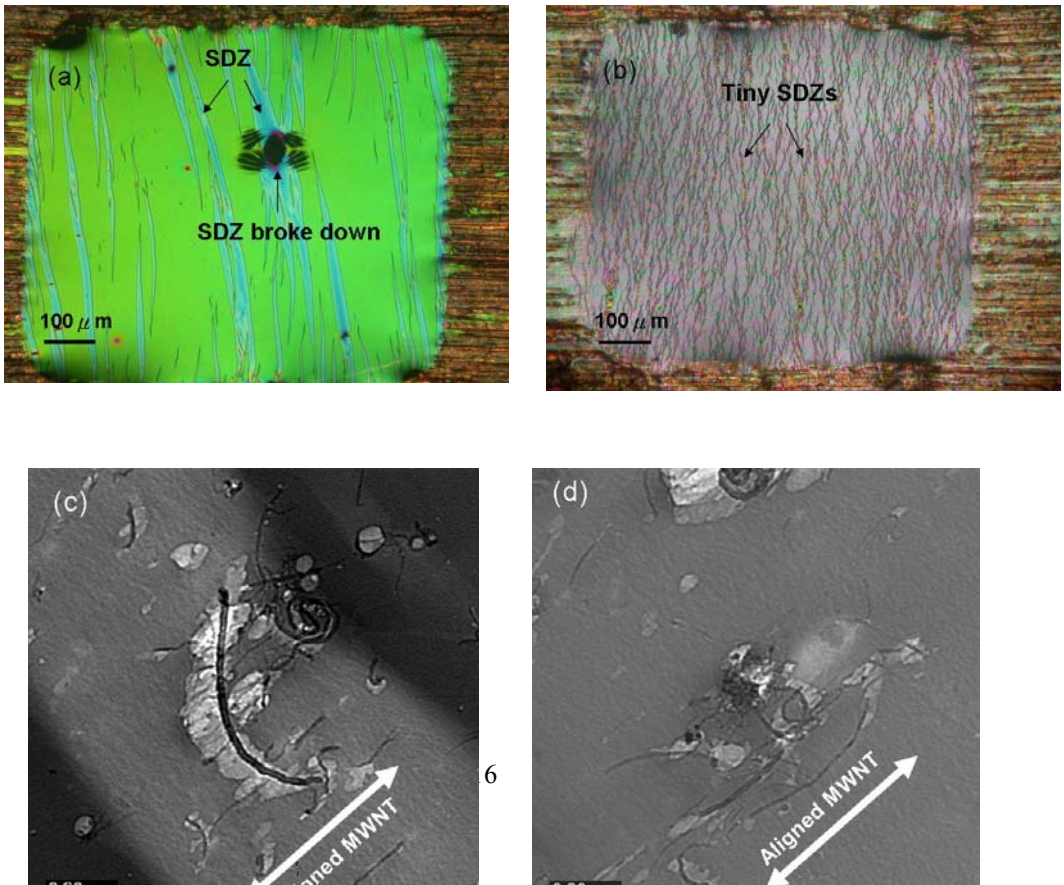

Figure 7. Optical micrograph of stretched (a) pristine PPO films, (b) MWCNTs/PPO composite film (weight fraction of MWCNT is 1.5 wt%), and (c)TEM micrographs of narrow SDZ, and (d) TEM micrograph of a wider SDZ in MWCNT/PPO films (weight fraction of MWCNT = 1.5 wt%).

The micro-necking characteristic of the SDZs was examined for the MWCNTs/PPO films and it was found that the *d* versis w curve generally followed that of the SDZs in the neat PPO but the depression appeared to be slightly lower than that in the neat resin for MWCNTs content of 1.5wt.% (Figure 8a). On the other hand, at higher MWCNTs contents (2.4 wt%) films, the depression became half of pristine PPO film. This effect due to MWCNTs dramatically increased the viscosity of PPO, thus the SDZ in MWCNTs/PPO film became hard than pristine PPO film and lead to depression depth of SDZ early reached saturation. The local distributions of stress and strain across the SDZ were analyzed from the AFM topography to reveal the micromechanics involved during the ductile microdeformation. For quantitative analysis on the restricted widening of SDZ, the chain friction coefficient during SDZ widening was also calculated by using a Rouse chain model. For a single PPO chain in the tube, the confining tube (A_{tube}) is approximately 0.55 nm^2 and in average a total of 23 chains share the tube space. Figure 8c shows the chain sliding velocity along the tube (v) in pristine PPO and MWCNTs/PPO films, the v were randomly distribution between the 1100~1900 nm/s. However, the total friction coefficient of pristine PPO can also be calculated from the Eqs. (2-3) and the data in Figure 8c. The Figure 8d shows the total friction coefficient of a PPO chain vs width of SDZ in pristine PPO and MWCNTs/PPO films. In the pristine PPO films, the friction coefficient increased with SDZ width w, until $w \sim w_c$ the friction coefficient became a constant, that gives the friction coefficient of pristine PPO ($\zeta_{PPO\text{-}PPO}$) to be $\zeta_{PPO\text{-}PPO} \sim 4.3 \times 10^{-5}$ k g/s. On the other

hand, In MWCNTs/PPO films the friction coefficient was also increased with SDZ width w and saturated at $w \sim w_c$, that gives the friction coefficient (ζ_T) for sample of 1.5 wt% MWCNTs to be $\zeta_T \sim 7.5 \times 10^{-5}$ k g/s. It strongly indicated that by the MWCNT networks embedded in the PPO film had dramatically increased the hardness of the ductile polymer and lead to high chain friction coefficient in MWCNTs/PPO films.

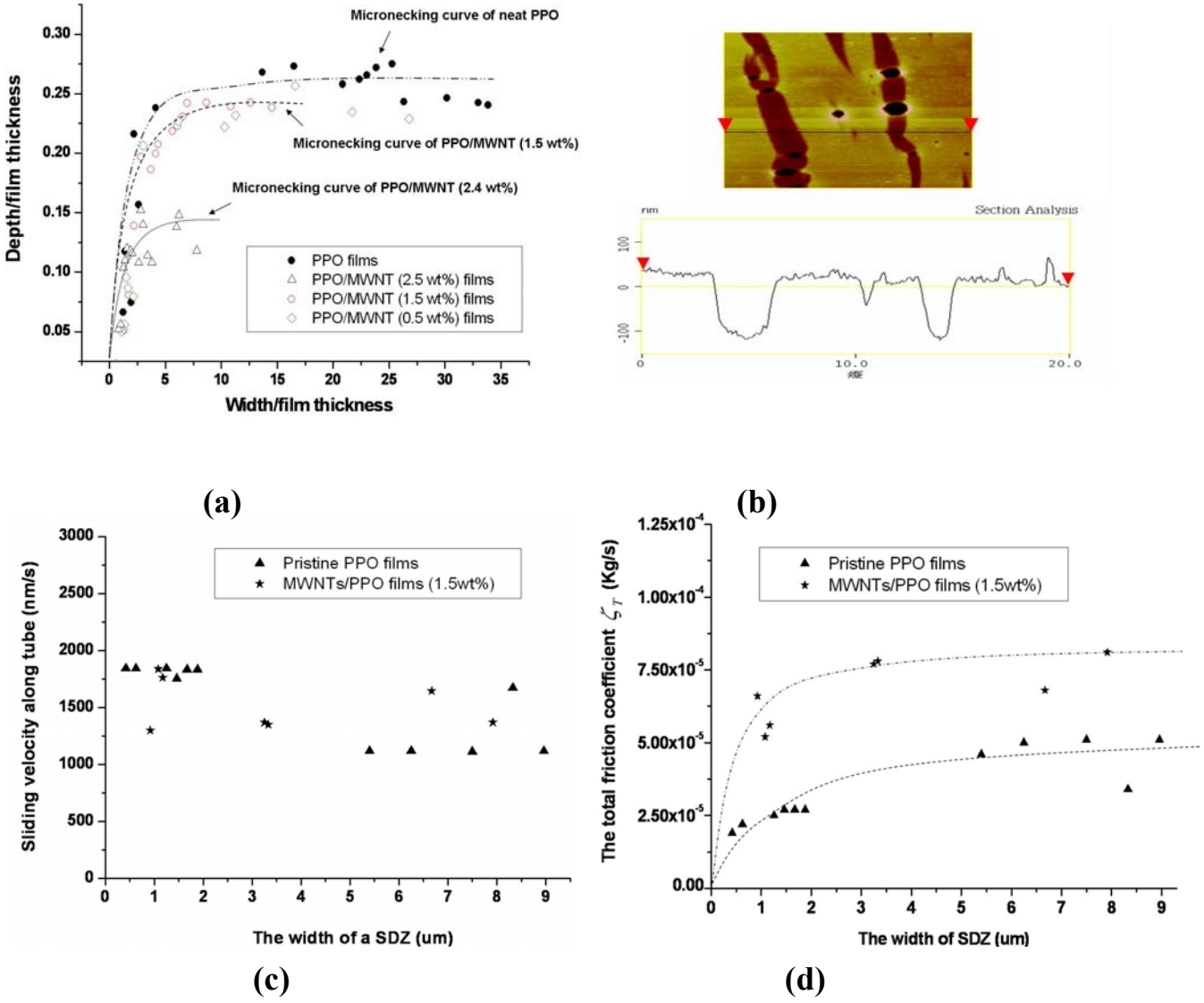

Figure 8. (a) SDZ depth vs SDZ width in the pristine PPO and MWNTs/PPO films, and (b) AFM micrograph of stretched and etched MWNTs/PPO film. (c) the sliding velocity of a PPO chain vs width of SDZ in pristine PPO and MWCNT/PPO films, and (d) the total friction coefficient of a PPO chain vs width of SDZ in pristine PPO

and MWCNT/PPO films.

The effect due to properties of the entanglement network

It is intriguing that the MWCNTs were drawn to the SDZ but not into the craze. Obviously, it has to do with the plastic flow of the polymer incurred during crazing or micro shear deformation. As revealed before, the local strain rate induced by the plastic flow of microdeformation always manifested a two-stage dependence on the strain [27]. For the first stage, the strain rate increases as the material is drawn into the local deformation zones. It is due to that the material deformation was accelerated during the straining and showed strain softening. The first stage stopped at a critical strain ε_h after which the strain rate decreased, illustrating a strain hardening that finally weaned any further deformation of the drawn polymer such that a constant draw ratio was maintained. The strain with the maximum strain rate is termed the hardening strain (ε_h), and it is related to the entanglement density of the chain entanglement network. The ε_h can be determined from micromechanical analysis of local deformation zones [27].

The entanglement density of the chain network ν_e not only has a strong influence on the value of the hardening strain ε_h, but also decides which mode of the microdeformations of crazing or shear yielding is the one to dominate the plastic flow. The PPO has a tight entanglement chain network (ν_e = 1.5×10^{26} chains/m^3) whilst the entanglement network of PS is much looser (ν_e = 3.3×10^{25} chains/m^3), as shown schematically in Figure 9a. Therefore, the hardening strains ε_h's for crazing in the loose chain network of PS and that for SDZs in the tighter PPO chain network are quite different. The hardening strain of PS of molar mass 2M g was determined to be ε_h = 1.4, and was approximately ε_h = 0.3 for PPO [27]. With this, the drawing mechanics of the plastic flow was analyzed in Figure 9b where the maximum strain ε_p (the plateau strain) was plotted against the width of the local deformation zones for both PS and PPO. Although the plateau strains ε_p's for both PS and PPO increase monotonically with the width of the deformation zones, the plateau strain for PS crazes is smaller than the hardening strain (ε_h = 1.4) of PS chain network for w < 5 μm. Recalled that virtually all the crazes found in the MWCNTs/PS films were thinner than 2 μm in width,

implying that the drawn PS chains in the crazes were still in the strain softening stage. Given that the MWCNTs are rigid, drawing of the MWCNTs into crazes with the softening chains, however, does appear vulnerable. On the contrary, the plateau strain in the SDZs has surpassed the hardening strain of the PPO chain network (ε_h = 0.3) for SDZs as narrow as 0.6 μm, a criterion by which the majority of the SDZs in the nanocomposite MWCNTs/PPO are strain-hardening. Thus, the chains in the plastic flow were capable to drag the MWCNTs into the local deformation zones.

By this simple view in terms of the structure of entanglement network and the micromechanics of the plastic flow of deformation zones in glassy polymers, the interactions between the embedded MWCNTs and the polymer chains can be understood in a coherent view. The complicated effect of filler arising from introducing MWCNTs into glassy polymers probably can be comprehended with the insight provided by this approach. There are still remaining issues left unanswered owing to the limited scope of this work. For example, the effect of single-walled carbon nanotubes and the mechanical properties of MWCNT/polymer nanocomposites of high MWCNT fractions which, however, will be explored later.

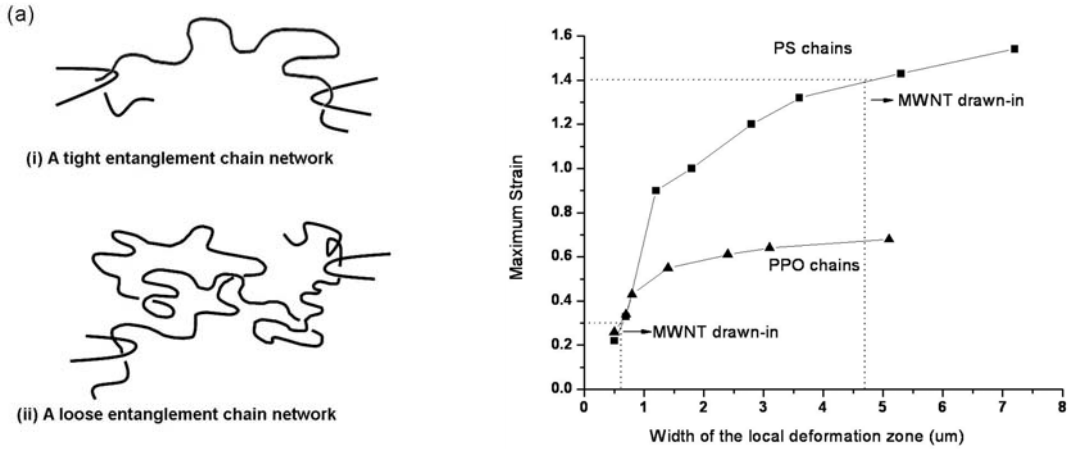

(a) (b)

Figure 9. (a) schematics of a tight polymer chain network and a loose chain network, and (b) the maximum strain versus the width of local deformation zones.

1-4 Conclusions

The MWCNTs network dramatically toughens the embedded brittle (PS) polymer by restricting micro-necking, leading to strain delocalization even after the initiation of microdeformation zones. But they were shown different micromechanical interaction between the MWCNTs and different type of polymer chains. In brittle polymers, the PS has a loose entanglement chain network and high hardening stain. Therefore, when crazing at the narrow width region the stain softening dominated leading to large difference in rigidity between MWCNTs and PS chains, thus the MWCNTs cannot be drawn into crazes. In addition, the MWCNTs were piled up at craze boundaries and increasing the drawing stress of crazing. Eventually discouraging the formation of crazes and leading to embrittleness at high MWCNTs content polymer films. Although the addition of MWCNTs increased the drawing stress of the shear zone, creating the similar effect of delocalization of strain and mild toughening, the MWCNTs were drawn into the shear zone. A tight entanglement chain network and low hardening stain in the ductile polymers. Hence, the stain hardening easily occurred in PPO films and drawn rigid MWCNTs into the SDZ.

1-5 References

(1) Yu, M. F.; Lourie, O.; Dyer, M. J.; Moloni, K.; Kelly, T. F.; Ruoff, R. S. *Science* **2000**, 287, 637.

(2) Hwang, G. L.; Hwang, K. C. *Nano Lett*. **2001**, 1, 435.

(3) Yakobson, B. I.; Campbell, M. P.; Brabec, C. J.; Bernholc, J. *Comput. Mater. Sci.* **1997**, 8, 341.

(4) Yang, Y.; Gupta, M. C.; Dudley K. L.; Lawrence R. W. *Nano Lett*. **2001**, 5, 2131.

(5) Hill, D. E.; Lin, Y.; Rao, A. M.; Allard, L. F.; Sun, Y. P. *Macromolecules* **2002**, 35, 9466.

(6) Liu, C. H.; Fan, S. S. *Appl. Phys. Lett.* **2005**, 86, 123106 1.

(7) Qian, D.; Dickey, E. C. *Appl. Phys. Lett.* **2000**, 76, 2868.

(8) Blond, D; Barron, V.; Ruether, M.; Ryan, K. P.; Nicolosi, V.; Blau, W. J.; Coleman, J. N. *Adv. Funct. Mater.* **2006**, 16, 1608.

(9) Hwang, G. L. ; Shieh, Y. T.; Hwang, K. C. *Adv. Funct. Mater.* **2004**, 14, 487.

(10) Coleman, J. N.; Cadek, M.; Blake, R.; Nicolosi, V.; Ryan, K. P.; Belton, C.; Fonseca, A .; Nagy, J. B.; Gun'ko, Y. K.; Blau, W.J. *Adv. Funct. Mater.* **2004**, 14, 791.

(11) Singh, S.; Pei, Y.; Miller, R.; Sundararajan, P, R.; *Adv. Funct. Mater.* **2003**, 13, 868.

(12) Zhu, J.; Kim, J.; Peng, H.; Margrave, J. L.; Khabashesku, V. N.; Barrera, E. V. *Nano Lett*. **2003**, 3, 1107.

(13) Li, X.; Gao, H.; Scrivens, W. A.; Fei, D.; Xu, Xiaoyou, Sutton, M. A.; Reynolds, A. P.; Myrick, M. L. *Nanotechnology* **2004**, 15, 1416.

(14) Qian, D.; Dickey, E. C. *J. Micro.* **2001**, 204, 39.

(15) Watts, P. C. P.; Hsu, W. K. *Nanotechnology* **2003**, 14, L7.

(16) Liu, T. X.; Phang, I. Y.; Shen, L.; Chow, S. Y.; Zhang, W. D. *Macromolecules* **2004**, 37, 7214.

(17) Zhang, W. D.; Shen, L.; Phang, I. Y.; Liu, T. X. *Macromolecules* **2004**, 37, 256.

(18) Manchado, M. A.; Valetini, L.; Biagiotti, J.; Kenny, J. M. *Carbon* **2005**, 43, 1499.

(19) Meincke, O.; Kaempfer, D.; Weickmann, H.; Friedrich, C.; Vathauer, M.; Warth, H. *Polymer* **2004**, 45, 739.

(20) Yang, A. C. M, Wang, R. C., Lin, J. H.; *Polymer*, **1996**, 37, 5751

(21) Hsiao, C. C.; Lin, T. S.; Cheng, L. Y.; Ma, C. C. M.; Yang, A. C. M. *Macromolecules* **2005**, 38, 4811.

(22) Lin, T. S.; Cheng, L. Y.; Hsiao, C. C.; Yang, A. C. M. *Mater. Chem. Phys.* ***2005,*** 94, 438.

(23) Kong, H.; Gao, C.; Yan, D. Macromolecules, **2004**, 37, 4022.

(24) Yang, A. C. M.; Kramer E. J.; Kuo, C. C.; Phoenix, S. L. *Macromolecules* **1986**, 19, 2010.

(25) Yang, A. C. M.; Kramer E. J.; Kuo, C. C.; Phoenix, S. L. *Macromolecules* **1986**, 19, 2020.

(26) Yang, A. C. M.; Kunz, M. S.; Logan, J. A. *Macromolecules* **1993**, 26, 1776.

(27) Lin, J. H.; Yang, A. C. M. *Macromolecules* **2001**, 34, 3698.

(28) Lin, C. H.; Yang, A. C. M. *Macromolecules* **2001**, 34, 4865.

(29) Kramer, E. J. *Adv. Polym. Sci.* **1983**, 52/53, 1.

(30) Donald, A. M.; Kramer E. J. *Polymer* **1982**, 23, 457.

(31) Yang, A. C. M.; Kramer E. J.; Kuo, C. C.; Phoenix, S. L. *Macromolecules* **1986**, 19, 2010.

(32) Yang, A. C. M.; Kramer E. J.; Kuo, C. C.; Phoenix, S. L. *Macromolecules* **1986**, 19, 2020.

(33) Donald, A. M.; Kramer E. J. *Mater. Scie.* **1982**, 17, 1871.

(34) Donald, A. M.; Kramer E. J. *Mater. Scie.* **1981**, 16, 2967.

(35) Donald, A. M.; Kramer E. J. *Mater. Scie.* **1981**, 16, 2977.

(36) Donald, A. M.; Kramer E. J. *Polymer* **1982**, 23, 461.

(37) Donald, A. M.; Kramer E. J. *Polymer* **1982**, 23, 1183.

(38) The area of the confining tube ($A_{polymer\ tube}$) for a single PS chain was calculated by following equation: $A_{polymer\ tube} = \frac{M_0}{N_{Av}\rho\, b}$
Where M_0 is the molar mass of a Kuhn monomer, N_{Av} is Avogadro's number, ρ is the density and b is the Kuhn length.

(39) We assumed a mass in a polymer random coil at chain end and let it move to another chain end. Thus the straight line distance is the end-to-end distance of polymer chain (R) and $R=bN^{1/2}$. But the mass undergo real distance is referred to the contour length of the chain (l) and l=bN. Therefore, the real velocity of polymer chain is revised for $\vec{v}$ = velocity of straight line $\times N^{1/2}$.

(40) Berger, L. L.; Kramer E. J. *Macromolecules* **1987**, 20, 1980.

(41) Cotiuga, I.; Picchioni, F.; Agarwal, U. S.; Wouters, D.; Loos, J.; Lemstra, P. *Macromol. Rapid. Commun.* **2006**, 27, 1073.

(42) M. Doi, S. F. Edward, "*the theory of Polymer Dynamics*", Clarendon, Oxford **1986**, p.338.

Chapter 2

Reinforcement of rigid-rod poly(p-phenylene benzobisoxazole) thin films by surface grafted carbon nanotubes

Abstract

Thin films of rigid-rod (Polybenzoxazole;PBO) polymer were prepared in poly(phsphric acid) (PPA) by one-step method. The microdeformation behaviors of the thin films were probed by using OM and TEM. In the stretching pristine PBO films, the crazing behavior was shown in PBO films and following the micronecking process. The crazes initiation at approximation 0.5% strain and the craze were unstable, widening as the strain increased. As strain increased further, local fibril breakdowns with the crazes began at approximately 2% strain. On the other hand, addition of multiwalled carbon nanotubes (MWNTs) grafted PBO chains in PBO films, does not improve much the mechanical toughness, however, strain delocalization induced by MWNTs, was observed. When Pyreneburtic acid treated SWNTs were added, a clear reinforcement effect was observed. The result shown that the median strain (ε_b) of SWNTs/PBO films containing 3 wt.% SWNTs was approximately 5 times higher than pristine PBO film. In addition, from TEM observation the SWNTs were observed in the crazed regions. This result revealed that the SWNTs were soft enough to participate in the crazing process, and increasing the craze fibril stability. On the other hand, the craze fibril stability can be prediction by the Weibull distribution and result also shows the craze fibril stability significantly increased by added SWNTs in PBO films.

2-1 Introduction

Polybenzoxazoles (PBOs) as a class of hetercyclic polymers has been developed originally by US Air Force researchers [1]. The PBOs and their fiber are shown excellent thermal stability (Decomposition Temperature (T_d) ~ 650C), chemical resistance and high Young's modulus (~ 270 GPa , > steel fibers) [1-4]. However, it is brittle due to very low elongation at break (ε_b ~ 2-3%). In generally, PBO can be synthesized in two fashions: (1).one-step: polymerization of

bis(o-aminophenol)s with aromatic diacid in poly(phsphric acid) (PPA) [3,5-6]. (2).Two-step:polymerization of bis(o-aminophenol)s with aromatic diacid chlorides in polar aprotic solvents [7-10]. one step method is easier for making high molecular weight PBO, PBO only dissolves in strong acid such as sulfonic acid, making the subsequent material processing (blending, grafting, molding) very difficult. Two-step polymerization process for PBO in which the flexible polyhydroxyamide (PHA) was first synthesized and then thermally converted into PBO. Recently, Kumar et al. [11] made composites of singlewalled carbon nanotubes (SWNTs) in PBO and spun into fibers by dry-jet wet spinning. The result shows the tensile strength of PBO fiber increased by about 50% on addition 10 wt.% of SWNT. That due to the carbon nanotubes (CNTs) have many outstanding physical properties such as small size (small diameter:0.4~5nm; long length: several μm, even to several mm), high Young's modulus (nearly 1 TPa) [12-13], high fracture strains (estimated to be 10-30%)[4], flexible (bending up to 120 degree). In addition, the CNTs are also considered to be ideal filler for reinforce other polymers [14-19]. On the other hand, the CNTs/PBO nanocomposite films were also been prepared by Bai et al.[20], they used fully conjugated PBO blending with multiwalled carbon nanotubes (MWNTs) in an aprotic Lewis acid solvent and fabricated the MWNTs/PBO films by spinning coating following preparation as light emitting diodes device. The MWNTs/PBO film shows excellent electroluminescence properties. However, the mechanical properties of PBO and CNTs/PBO films were unexplored before. In this study, the PBO and CNTs (SWNTs and MWNTs)/PBO nanocomposite films were prepared, as well as their micromechanical properties were also characterized. In addition, for the CNTs can be dispersed well into the PBO matrix, the covalent functionalization (for MWNTs) and noncovalent functionalization (for SWNTs) methods were used.

2-2 Experimental section

Materials

The MWNTs and SWNTs were purchased from DESUN Nano Company (Taiwan). 2,2-bis(3amino-4-aminophenol)hexafluoropropane (BisAPAF), 4,6-diaminoresorcinal dihyrochloride (DAR), isophthaloyl chloride (IC),

terephthaloyl chloride (TC), anhydrous N-methylpyrrolidone (NMP), 1-pyrenebutyric acid (pyrene-COOH) , poly(phosphoric acid) (PPA) and P_2O_5 were obtained from Aldrich and used without further purification.

Synthesis of PBO

The pristine PBO can be synthesized by one step polymerization in poly(phsphric acid). Here, we modified the method of Kumar et al. [11]. 1,4-diaminoresorcinol dihydrochloride (DAR) (852.24 mg,0.004 mol), terephthaloyl chloride (TC) (812.1 mg, 0.004 mol), and 2.494 g of phosphoric acid (85%) were pour into a glass flask equipped with a mechanical stirrer and nitrogen inlet/outlet. The mixture was heating at 65 °C for 16 h and subsequently heating at 80 °C for 4 h to incorporate the P_2O_5 (1.608 g) and then kept at 80 °C for another 2 h. After 2 h, further P_2O_5 (1.43 g) was added to the mixture and the polymer content is 23wt %. The polymerization was then slowly increased to 160 °C for 16 h with constant stirring. Finally the mixture was heated to 190 °C for an additional 4 days while stirring and then the polymer solution precipitated (Scheme 1), washed in deionized water, and dried under vacuum at 100 °C for 24 h. The intrinsic viscosity value of PBO is 61 dL/g (Mv ≈ 43,000 determinate by Mark-Houwink eq [21]) determined in methanesulfonic acid at 30 °C .

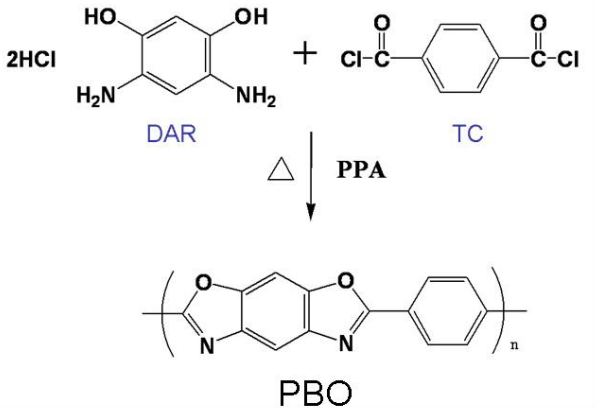

Scheme 1. Synthesis of PBO by one step polymerization.

Synthesis of PBO-graft-MWNT (PBO-g-MWNTs) and Preparation of

PBO-g-MWNTs/PBO film.

The PBO surface grafting on the MWNTs can be preparation by two step method [8], 377.58 mg (1mmole) of 2,2-bis(3amino-4-aminophenol) hexafluoropropane (BisAPAF), 162.89 mg (2mmole) of anhydrous pyridine and 4 ml of anhydrous NMP were added to a dry 25ml glass flask equipped with a nitrogen inlet and mechanical stirrer. After the BisAPAF was completely dissolved, the solution was cooled to 5□ in an ice/water bath and isophthaloyl chloride (IC) (203.12mg, 0.98mmole) was added slowly to the solution. The reaction mixture was stirred at room temperature for 16 h to form BisAPAF terminated PHA prepolymer.

On the other hand, the pristine multi-walled carbon nanotubes (MWNTs) were refluxed in concentrated nitric acid/sulfuric acid, then washed thoroughly with deionized water and dried completely and obtained the anchoring carboxylic acid groups onto the tube external surfaces (MWNTs–COOH) [22]. The MWNTs–COOH were converted to acylchloride (MWNT-COCl) in $SOCl_2$ at 40 □ for 8 h. And then add MWNT-COCl into the reactor and reacted with BisAPAF terminated PHA prepolymer at room temperature for 16 h (Scheme 2). The resulting viscous solution was washed in NMP by sonication and then vacuum-filtered through a 0.2μm PTFE membrane, to remove free polymer. The surface grafting of PHA can be converted into PBO upon subsequent heating at 350 □ 8hr. The PBO-grafted MWNTs were mixed, by approximately 3 wt % in weight, with the PBO in PPA solution. The PBO-g-MWNTs/PBO films were spun cast from the solution, and the film thickness was controlled to be around 0.5μm. The PBO-MWNTs/PBO film was floated off the substrate on distilled water and removed PPA. Then the film bonded onto supporting copper grids. After following the proper bonding procedure, the specimen was mounted in a strain jig and stretched under an optical microscope to observe the growth of local deformation zones [23-27].

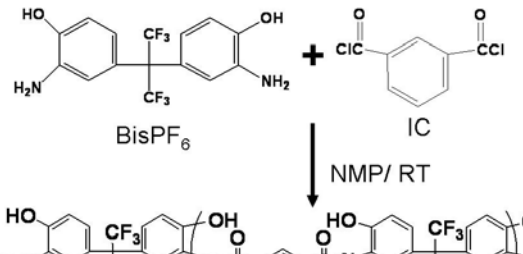

Scheme 2. Synthesis of PHA grafted-MWNT via two steps polymerization.

Preparation of Noncovalent Functionalization of SWNTs by aromatic interaction (Pyrene-SWNTs) and Pyrene-SWNTs/PBO Composite Films.

The non-covalent binding of pyrene groups on the surface of CNTs and improved dispersion properties of CNTs in common solvent has been observed [28]. In a typical experiment, equal weight of 1-pyrenebutyric acid and SWNTs was incubated in PPA (0.5 mg/ml) solution and stirred for 8 h at 120□. After 8 h, the mixture was mixed with PBO and then the pyrene-SWNTs/PBO solution slowly increased to 160 °C for 24 h with constant stirring. The pyrene-SWNTs/PBO films were spun cast from the solution, and the film thickness was controlled to be around 1.5 μm. Then the film bonded onto supporting copper grids before stretching (Scheme 3).

Transmission electron microscopy (TEM, JEOL JEM-2010) was used to observe the microstructures of the CNT/Polymer films. Thermal gravimetric analyzer (TGA, Perkin-Elmer thermal analysis TG/DTA) was used to determinate the amount of PBO grafted on the MWNTs. The chemical structure of PHA and PBO were detected by Fourier-Transform Infrared spectroscopy (FT-IR) which recorded between 4000 and 400 cm^{-1} on a Bomem DA8.3 infrared spectrophotomete.

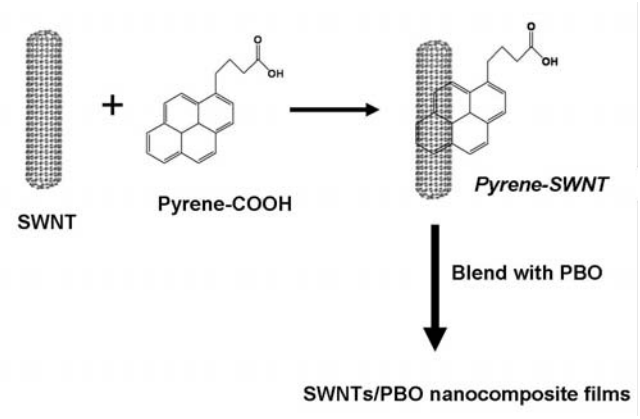

Scheme 3. Synthesis of Pyrene-SWNTs.

2-3 Results and Discussions

Microstructure of Local deformation zone in PBO films.

Local deformation zones (includes both crazes and shear deformation zone) are commonly observed in deformed in glassy polymers and initiated upon stretching. Crazes are crack-like defect that are load-bearing and fibrillated in zone. It thickness by drawing more polymer in from the edge of the zone, generally occurred in a brittle polymer [29-30]. On the other hand, shear deformation zones (SDZs) are similar to the craze, but SDZ is not fibrillated as in a craze. They are uniformly thinned in the zone and commonly observed in ductile polymer [27, 31]. However, the local deformation zones were as precursor of fracture. Because the interior local deformation zones break down, catastrophic fracture starts.

The rigid-rod PBO polymer films can be obtained by the condensation of 1,4-diaminoresorcinol dihydrochloride with terephthaloyl chloride, in the presence of poly(phosphoric acid) followed by spin casting. Figures 1a-g shows the pristine PBO films under stretched with an increase of strain. When the films were stretched, local deformation zones emerged in the films. The deformation zones were nucleated after 0.5% (ε_c) strain. As strain increased (at 0.8 % strain, Figure 1b) the fibrilous microstructure was generated. After strain increased further, local fibril started breakdowns within the deformation zones at approximately 1.8 % strain (Figure 1d), and the maximum strain of film cracking was at 3% (Figure 1g). This result was consistent with property of PBO fibers [11], and revealed the PBO

film was very brittle. The micro structure of the local deformation zones were examined under AFM (Figure 2a-b) and TEM (Figure 2c-d). The topography of the crazed PBO film (Figure 2a) was measured by AFM. The surface of the PBO film was generally rough, and the craze fibrils were aligned to the stretching direction (Figure 2b). For a typical craze in the PBO film, the surface profile obtained from AFM analysis and demonstrates a large depression in the deformation region. The maximum depth in the craze was found to increase linearly with the craze width, eventually reaching a saturated value at a critical width (w_c) around 3.5 μm, as shown in Figure 2c, apparently following the micronecking process. The TEM micrograph (Figures 2a-b) of PBO film shown the craze structure was different with typical brittle polymer (such as polystyrene) [32], the craze fibrils of PBO were revealed very short and wide due to a stiff molecular chain of PBO. Thus the PBO film under crazing, drawing of the rigid chain of PBO to form crazes is difficult and unstable. These crazes are likely to have grown from the “weak spots” of the materials.

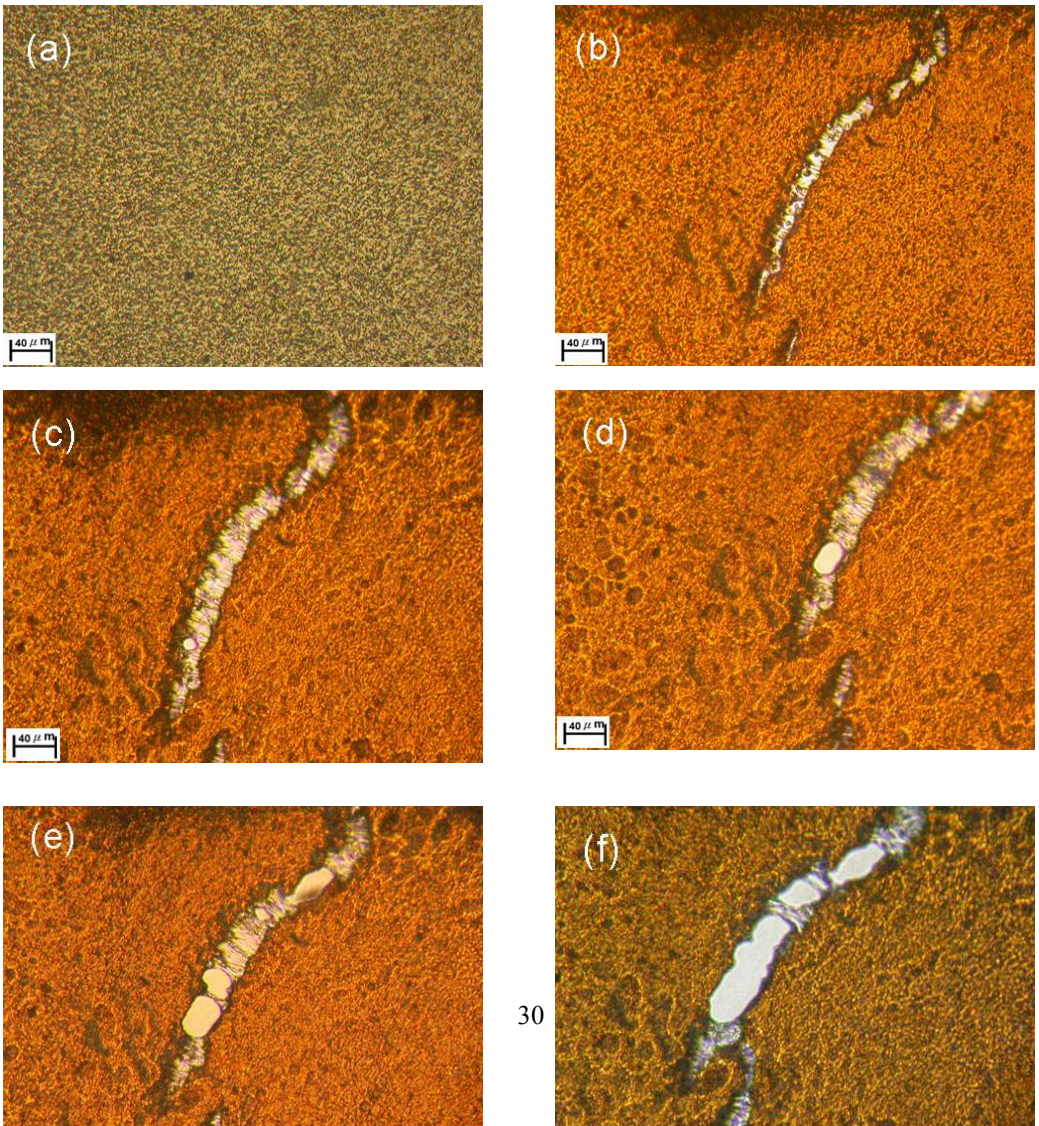

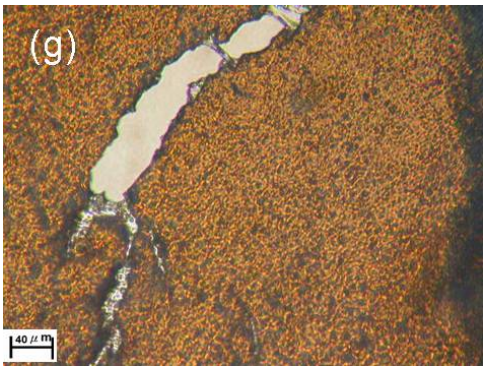

Figure 1. Optical micrograph of pristine PBO under stretching with different strains: (a) without stretching, (b) 0.8%, (c) 1.5%, (d) 1.8%, (e) 2.2%, (f) 2.6%,and (g) 3.0%.

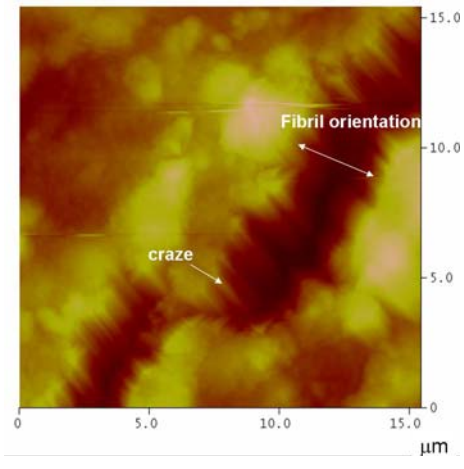

(a)

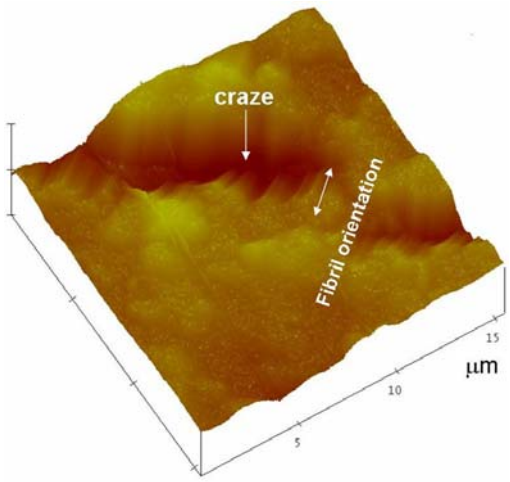

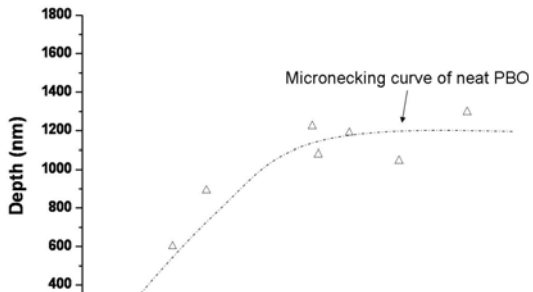

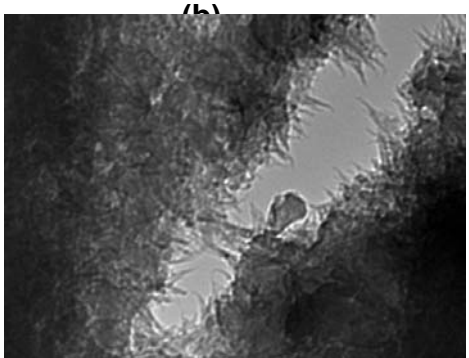

(c) **(d)**

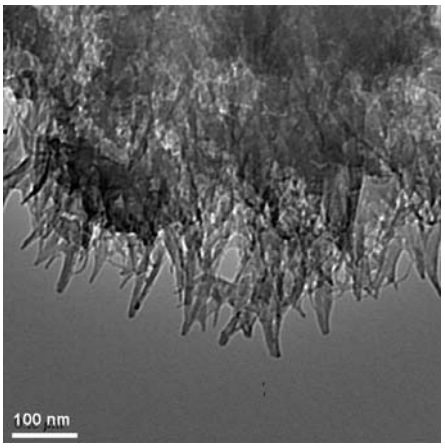

(e)

Figure 2. (a) AFM micrograph of stretched PBO films, (b)Craze surface topography in pristine PBO films, (c) craze depth *d* vs. craze width *w* in the PBO films, (d) TEM craze filbrils of pristine PBO films Lower and (e) higher magnification.

Synthesis of PBO-graft-MWNT (PBO-g-MWNTs) and modified Craze morphology.

The MWNTs were first surface grafted with PHA/PBO chain to impart good interface compatibility and dispersion properties into the PBO matrix. Fourier-Transform Infrared spectroscopy (FTIR) was used to identify the existence of PHA grafted on the MWNTs (Figure 3). After graft polymerization, new peaks were observed emerging in the frequency range from 2800 cm^{-1} to 3200 cm^{-1} that contained absorptions due to sp^2 (=C-H) bond stretching (3000 ~ 3200 cm^{-1}) of MWNTs. Hydroxyl group (-OH) stretching (3400 ~ 3100 cm^{-1}) and strong carbonyl (-C=O) group absorption at 1650 cm^{-1}[8]. both being clear evidence for PHA grafting on the MWNTs. After heating at 350 □ 8hr the PHA grafted MWNT can be

converted into PBO grafted MWNT. The fine nanostructure of PBO grafted MWNT was measured by transmission electron microscopy. As shown in Figure 4a, the MWNTs are wrapped by PBO chains can be observed. In addition, the PBO-g-MWNT can well disperse in PPA (figure 4b). On the other hand, from the TGA data (at heating rate of 10 □/min from RT to 800 □ under a N_2 atmosphere, Figure 4c), the difference in the residual weight loss at 800 □ between MWNT-g-PBO (49 wt.%), pristine PBO (60 wt.%) and MWNT-COOH (78 wt.%) shows that the PBO graft amount to ~55 wt.% of total weight of the synthesized PBO-g-MWNT.

The micro-mechanical testing of MWNT/PBO (with 3 wt% loading of the MWNT in PBO) composite film was shown that, the strain of local fibril breakdowns slightly increase to 4%. This suggests that addition of PBO-g-MWNT does not improve much the mechanical toughness. Because for the rigid chain of PBO, the drawing stress of microdeformation is already high, thus MWNTs reinforce more mechanical properties of PBO films is not easily. However, contrary to the pristine PBO film (Figure 5a), strain delocalization induced by MWNTs was observed in MWNTs/PBO film (Figure 5b). On the other hand, the TEM observation (Figure 5c) shown that the MWNTs were rarely found at crazes boundaries. It was maybe due to the MWNTs are always too rigid to be drawn into the crazes and low fibril stability in PBO. Thus, the crazes were mainly initiated in the regions where MWNTs density was low. Therefore, MWNTs play very limited role in reinforcing. For this reason, the single wall carbon nanotubes (SWNTs) may be a good chose for reinforce polymer films intrinsically.

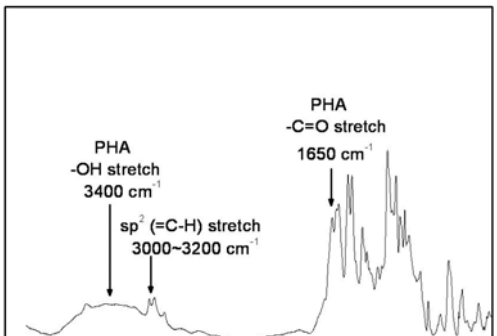

Figure 3. The FTIR spectra of the PBO and PBO-g-MWNT.

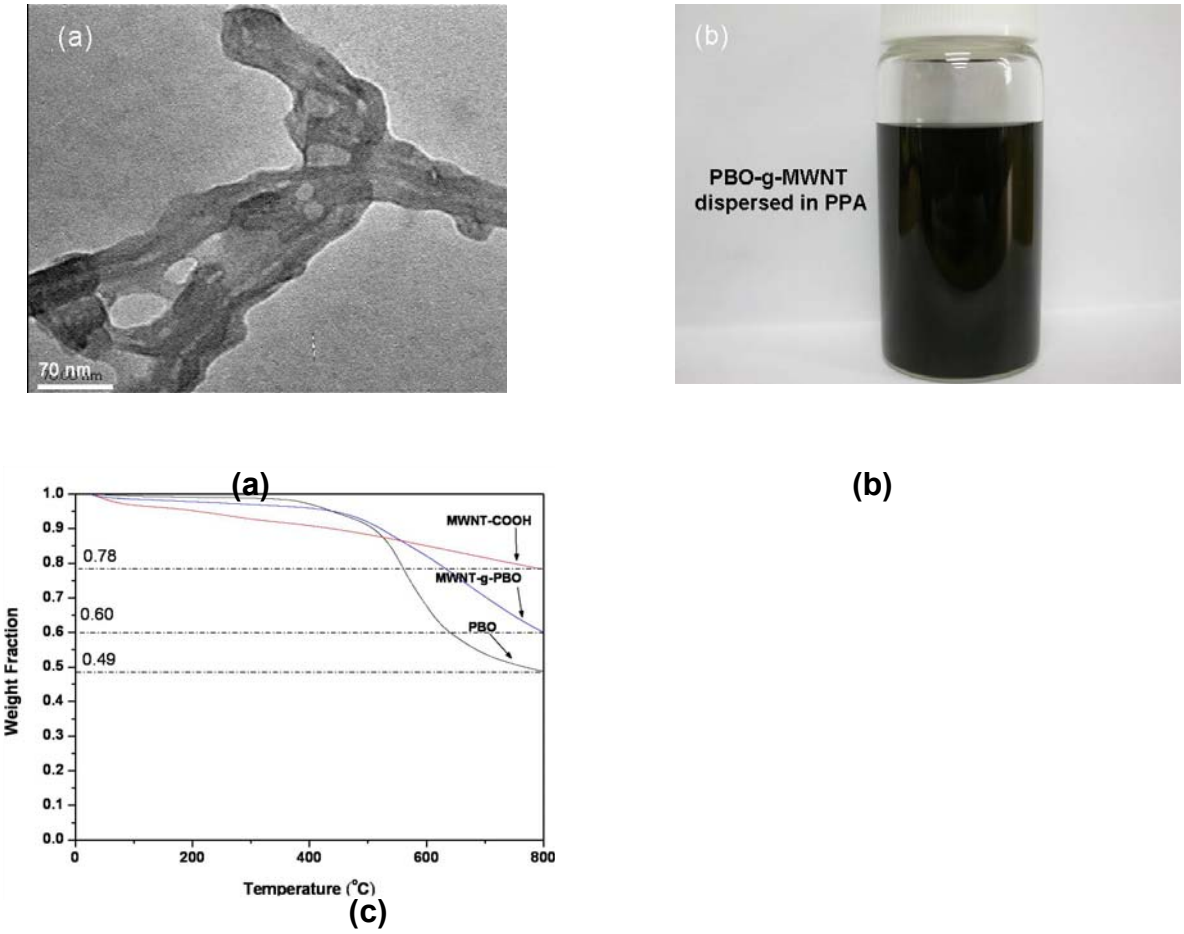

Figure 4. (a) TEM micrograph of PBO-g-MWNT,(b) The PBO-g-MWNT/PPA solution (c) TGA curves of the MWNT-COOH and PBO-g-MWNT.

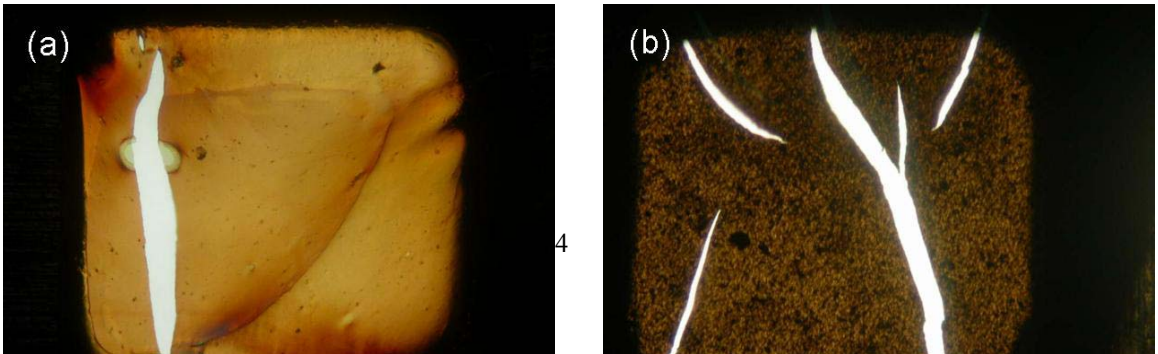

(a) **(b)**

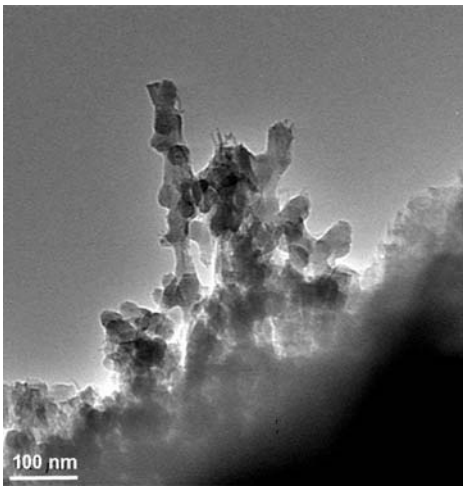

(c)

Figure 5. Optical micrograph of stretched (a) pristine PBO film at 3 % strain, (b) MWNT/PBO film (MWNT is 3 wt%) at 4 % strain. (c) TEM craze filbrils of MWNT/PBO films.

Interaction between of SWNTs and Crazes.

It is also interesting to investigate the SWNTs microdeformation interactions in rigid-rod polymer. Because of SWNTs have a high tensile strength, modulus and soft than MWNTs. SWNTs have short diameter (0.4~3 nm) [33] and this diameter range is roughly equal to the craze fibrils diameter, that imply SWNTs maybe can be drawn into the crazes. Nevertheless, SWNTs are not easy dispersion in polymer matrixes, due to they have strongly van der Waal force stemming from large surface areas. Non-covalent method is a favor way to functionalize SWNTs, because of non-covalent ways can preserve the SP^2 nanotube structure and their mechanical, electronic properties. here, we also used physical dispersing (π-π interaction) [28] to yield good dispersion of the SWNTs in PBO matrix. The

pyreneburtic acid as modifier, irreversiblely adsorbed onto the inherently hydrophobic surfaces of SWNTs in a poly(phosphoric acid) solution and stirring with PBO polymer. The microstructure of the local deformation zone was examined under TEM (Figure 6a), SWNTs were observed in the crazed regions. That was showing a different behavior than MWNT system, these results due to SWNTs were soft enough to participate in the crazing process and increasing the craze fibril stability. However, some small diameters of MWNTs were also observed in this condition due to impurity of SWNTs. In addition, the SMNTs/PBO composite film does not show strain delocalization (Figure 6b) as MWNTs/PBO system.

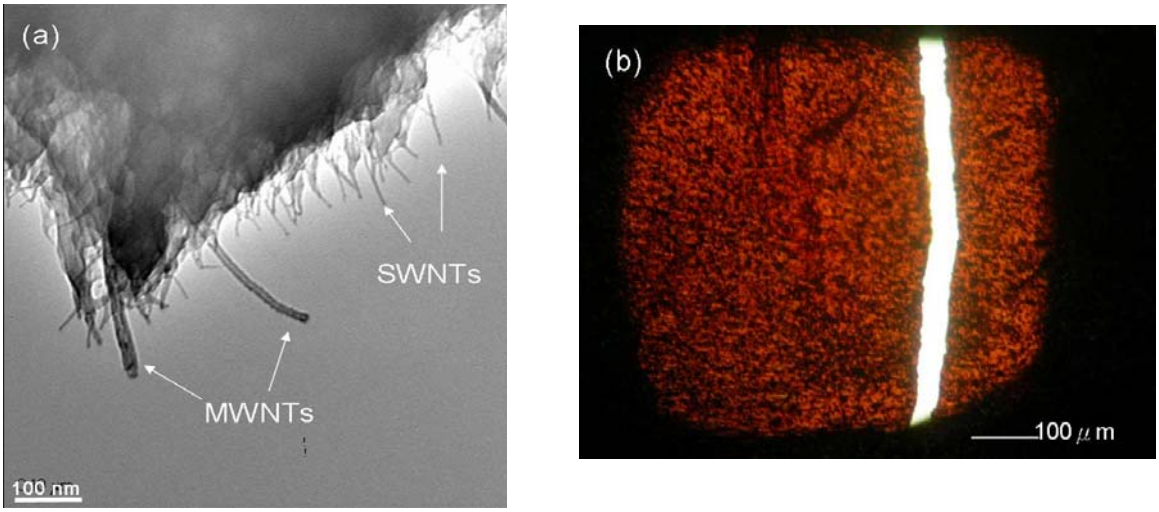

(a) **(b)**

Figure 6. (a) TEM craze filbrils of SWNT/PBO films, (b) Optical micrograph of stretched SWNT/PBO film (SWNT is 3 wt%) at 11 % strain.

Craze Breakdown Statistics.

The mechanisms of fibril breakdown are of crucial importance in the study of the fracture properties of glassy polymers. The fibril breakdown statistics have been investigated by examining simultaneously the failure events in a large number of independent films specimens and craze fibril stability are can be predicted by Weibull distribution [32]. Here, we also used this method to understand the probability of craze fibril breakdown in PBO and SWNT/PBO composite films. The cumulative number local fibril breakdown (p_b) of pristine PBO, MWNTs/PBO and

SWNTs/PBO films squares which had local fibril breakdown at various strains during the tensile test, as shown in Figure 7a. The full curve p_b provides useful information on the fibril breakdown statistics and will be explored later with a Weibull model. In addition, for the present we defined the median strains (ε_b) as p_b =0.5. The result shows, the ε_b of pristine PBO is 1.25 %. When MWNTs (3wt.%) added in PBO film, the ε_b slightly increased to 2.6 %. On the other hand, the median strain in SWNTs/PBO films (Figure 7b) were approximately 3~5 times (ε_b = 4.5 ~ 6.8 %) of that in pristine PBO film. The probability of craze fibril breakdown $p(\varepsilon_p)$ at a plastic strain ε_p (ε_p = grid strain ε - ε_c) is the Weibull distribution [32].

$$p(\varepsilon_p) = 1-\exp[-(V_0/V_b)(\varepsilon_p/\varepsilon_w)^{\rho}] \qquad (1)$$

where ε_w is the Weibull scale parameter, ρ is the Weibull modulus, V_0 is the initial grid square volume, and V_b is a volume in which one fibril breakdown will be encountered at reference stress of σ_b (for the large film squares we take V_0/V_b=1). Taking logarithms twice, one can write equation 1 in the form

$$\ln\{\ln[1/(1-p)]\} = \rho \ln(\varepsilon_p) - \rho \ln(\varepsilon_w) + \ln(V_0/V_b) \qquad (2)$$

The Weibull scale parameter ε_w and modulus ρ can be determined from the y intercept and the slope, respectively, of a plot of $\ln\{\ln[1/(1-p)]\}$ vs. $\ln(\varepsilon_p)$, the so called Weibull plot. The Figure 8a shows a typical Weibull plot for craze breakdown in PBO film. It is clearly indicated that craze fibril breakdown is well modeled by a Weibull distribution. In addition, the Weibull prediction median fibril breakdown strain (ε'_b) for etch squares can be determined by Weibull distribution (ρ and ε_w) for that group (N_g) and the value ε'_b is given from equation 1 as

$$\varepsilon'_b - \varepsilon_c = \varepsilon_w [(V_b/V_0) \ln 2/N_g]^{1/\rho} \qquad (3)$$

Figure 8b shows fibril stability ($\varepsilon'_b - \varepsilon_c$) versus various weight fraction of SWNT in PBO films. This result suggested that the craze fibril stability significantly increased by added SWNTs in PBO films and shown approximately 3 times at 3 wt% SWNT in PBO film. But at high SWNTs content (5 wt.% and 10 wt. %) condition, the fibril

stability were decreased due to SWNTs poor dispersion and/or aggregation occurred in PBO film.

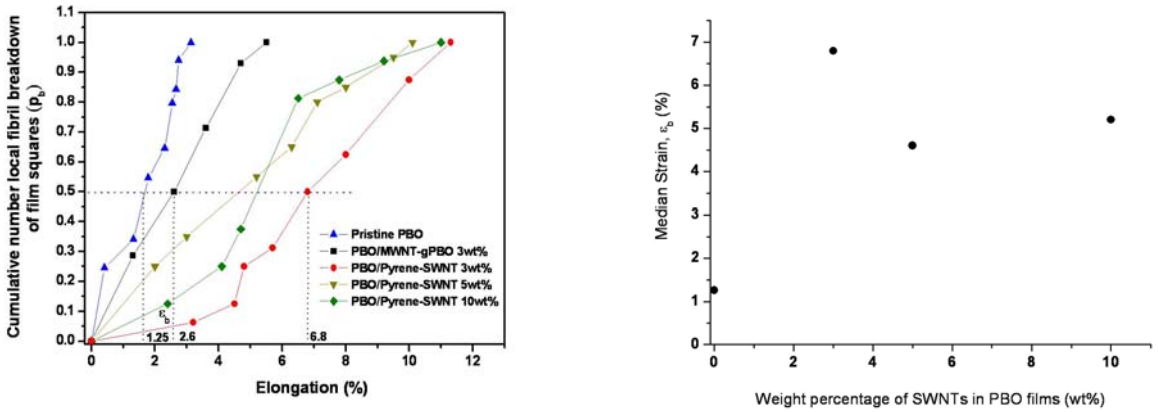

(a) **(b)**

Figure 7. (a) Cumulative number fraction of film squares vs tensile strain, (b) Median strains for fibril breakdown ε_b vs. SWNT loading.

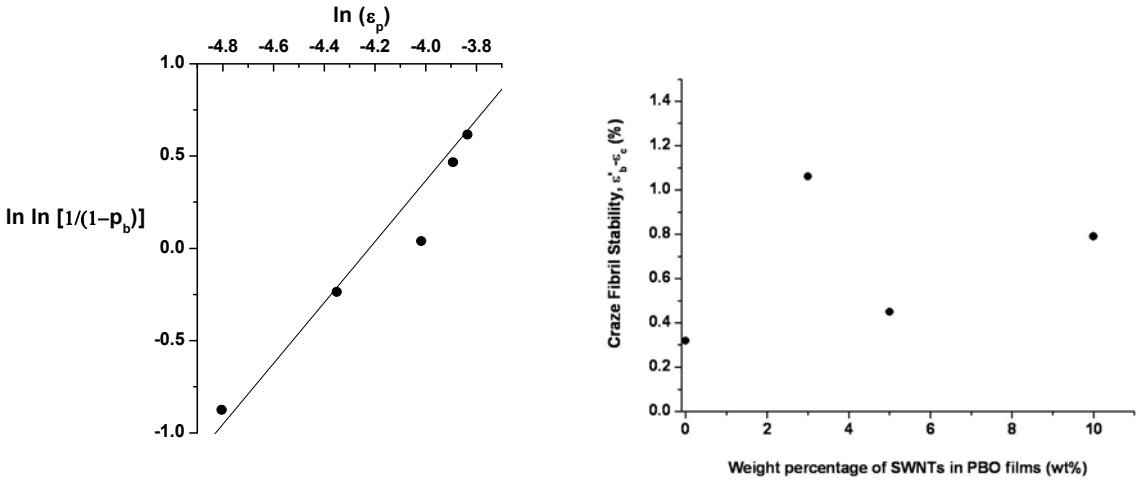

(a) **(b)**

Figure 8. (a) Typical Weibull polt, ln[ln(1/(1-p_b))], vs. ln ε_p for craze filbril breakdown in PBO films, (b) plot of fibril stability (ε_b- ε_c), vs various SWNT loading in composite films.

2-4 Conclusions

Thin PBO films were obtained by one-steps route in PPA and solution casting. The micro-deformation behavior of PBO films revealed that PBO is very hard, but can

be drawn into fibers and formed crazes. However, it is brittle due to very low elongation at break (~2%). On the other hand, the MWNTs surface grafted with PBO chains can well dispersed in PPA solution and PBO matrix. The MWNTs/PBO composite films were shown stain delocalization. However, for rigid-rod polymers, drawing stress of microdeformation is already high, thus MWNTs play very limited role in reinforcing. Pyreneburtic acid treated SWNTs were added, a clear reinforcement effect was observed. Because of SWNTs are softer and drawable along with the polymer chains in the process of microdeformation. On the other hand, the craze fibril stability of pristine PBO and SWNTs / PBO composite films can be predicted by Weibull distribution, the result shows the craze fibril stability significantly increased by added SWNTs in PBO films, demonstrating good prospect of reinforcing, even for rigid rod polymers.

2-5 References

(1) Ulrich, D. R. *Polymer,* **1987,** 28**,** 533.

(2) Chae, H. G.; Kumar, S. *J. Appl. Polym. Sci.* **2006**, 100, 791.

(3) Choe, E. W.; Kim, S. N. *Macromolecules*, **1981**, 14, 924.

(4) Davies, R. J.; Montes-Moran M. A. ; Riekel, C. ; Young, R. J. *J. Mater. Sci.* **2001**, 36, 3079.

(5) Wolfe, J. F.; Loo, B. H.; Arnold, F. E. *Macromolecules*, **1981**, 14, 915.

(6) So, Y. H.; Heeschen, J. P. *J. Org. Chem.* **1997**, 62, 3552

(7) Zhang, H.; Farris, R. J.; Westmoreland, P. R. *Macromolecules*, **2003**, 36, 3944.

(8) Hus, S. L. C.; Chang, K. C. ; *Polymer,* **2002,** 43**,** 4097.

(9) Chang, J. H.; Chen, M. J.; Farris R. J. *Polymer,* **1997,** 39**,** 5649.

(10) Hsiao, S. H.; Yu, C. H.; *Macromol. Chem. Phys.* **1998**, 199, 1247

(11) Kumar, S.; Dang,T. D.; Arnold, F. E.; Bhattacharyya, A. R.; Min, B. G. Zhang, X.; Vaia, R. A.; Park, C.; Adams, W. W.; Hauge, R. H.; Smalley, R. E.; Ramesh, S.; Willis, P. A. *Macromolecules*, **2002**, 35, 9039.

(12) Yu, M. F.; Lourie, O.; Dyer, M. J.; Moloni, K.; Kelly, T. F.; Ruoff, R. S. *Science* **2000**, 287, 637.

(13) Hwang, G. L.; Hwang, K. C. *Nano Lett*. **2001**, 1, 435.

(14) Coleman, J. N.; Cadek, M.; Blake, R.; Nicolosi, V.; Ryan, K. P.; Belton, C.; Fonseca, A .; Nagy, J. B.; Gun'ko, Y. K.; Blau, W.J. *Adv. Funct. Mater.* **2004**, 14, 791

(15) Blond, D; Barron, V.; Ruether, M.; Ryan, K. P.; Nicolosi, V.; Blau, W. J.; Coleman, J. N. *Adv. Funct. Mater.* **2006**, 16, 1608

(16) Hwang, G. L. ; Shieh, Y. T.; Hwang, K. C. *Adv. Funct. Mater.* **2004**, 14, 487.

(17) Coleman, J. N.; Khan, U.; Gun'ko, Y. K. *Adv. Mater.* **2006**, 18, 689.

(18) Hsiao, C. C.; Lin, T. S.; Cheng, L. Y.; Ma, C. C. M.; Yang, A. C. M. *Macromolecules* **2005**, 38, 4811.

(19) Schadler, L. S.; Giannaris, S. C.; Ajayan, P. M. *Appl. Phys. Lett.* **1998**, 73, 3482.

(20) Huang, J. W.; Bai, S. J. *Nanotechnology*, **2005**, 16, 1406

(21) Cotts, D. B.; Berry, G. C. Macromolecules, **1981**,14, 930.

(22) Lin, T. S.; Cheng, L. Y.; Hsiao, C. C.; Yang, A. C. M. *Mater. Chem. Phys.* ***2005,*** 94, 438.

(23) Yang, A. C. M.; Kramer E. J.; Kuo, C. C.; Phoenix, S. L. *Macromolecules* **1986**, 19, 2010.

(24) Yang, A. C. M.; Kramer E. J.; Kuo, C. C.; Phoenix, S. L. *Macromolecules* **1986**, 19, 2020.

(25) Yang, A. C. M.; Kunz, M. S.; Logan, J. A. *Macromolecules* **1993**, 26, 1776.

(26) Lin, J. H.; Yang, A. C. M. *Macromolecules* **2001**, 34, 3698.

(27) Lin, C. H.; Yang, A. C. M. *Macromolecules* **2001**, 34, 4865.

(28) Chen, R. J.; Zhang, Y.; Wang, D.; Dai, H. *J. Am. Chem. Soc.* **2001**, 123. 3838

(29) Kramer, E. J. *Adv. Polym. Sci.* **1983**, 52/53, 1.

(30) Donald, A. M.; Kramer E. J. *Polymer* **1982**, 23, 457.

(31) Yang, A. C. M.; Wang, R. C., Lin, J. H.; *Polymer*, **1996**, 37, 5751

(32) Yang, A. C. M.; Kramer, E. J. *Macromolecules* **1986**, 19, 2010.

(33) Baughman, R.H.; Zakhidov, A. A.; de Heer, W. A. *Science* **2002**, 297,78

Chapter 3

Electrical Properties of Thin Film of Carbon Nanotubes/Polymer Nanocomposites: Effects of Surface-grafting and π-π Stacking Modification

Abstract

In this study, electric conductive properties of multi-walled carbon nanotubes (MWNTs)/polymer nanocomposite was investigated in the percolating network system after improving dispersal of MWNTs as conductive fillers in the polymeric matrix via surface-grafting polystyrene (PS) and polybenzoxazole (PBO), and modification by means of π-π stacking without breaking sp^2 nanotube structure. The amounts of carboxyl groups on MWNTs through acid treatment and resistivity of MWNTs with various amounts of carboxyl groups were quantitatively determined. Resistivity decreases with weight fraction of functionalized MWNTs and the results confirm the percolation behavior. Surface grafted nanotubes can substantially reduce the electrical conductivity if the grafted polymer is an electrical insulator. For 3~5 vol-% of functionalized MWNTs content in PS-MWNTs/PS composites which MWNTs was grafted to PS, MWNTs in the composites formed a percolating network and the value of electric resistivity decreased sharply by 7 orders of magnitude and furthermore decreased by a factor of 10^6 by switching the grafting polymer from PS to PBO. The pyrene-functionalized MWNTs were prepared by employing π-π stacking via sonication and were blended with polyimide (PI) as a matrix, and the resistivity results indicate the great improvement in the electronic property due to more complete nanotube structure. The resistivities of these different MWNTs/polymer composites based on percolation theory are best fit and furthermore the contact resistance across two contacting CNTs can be evaluated.

3-1 Introduction

Ever since the initial discovery of carbon nanotubes (CNTs) in the 1991 [1], they had brought widespread research optimism for unveiling the fundamental properties, fabrication techniques, and novel applications. With great aspect ratios and excellent intrinsic conductive properties, CNTs have been attempted to use for a central filler to improve the conductivity in the insulating polymer matrix. [2] The well dispersed CNTs formed percolating networks in the MWNTs/polymer composites, and therefore they improved the electric conductivity effectively by forming an electric conducting tunnel. Z. Ounaies et al. [3] and Xiaowen Jiang et al. [2] dispersed CNTs into polyimide (PI), and the conductivity was measured from 10^4 to 10^2 S/cm.

However, owing to the strong van der Waals interaction, CNTs tend to form into aggregates resulting in poor dispersion in the polymeric matrix and negative effects on the properties of the composites. [4-15] Chemical functionalization via surface-grafting has been used for dispersion of CNTs in the polymer matrix. S. P. Li [9], Bao-Ku Zhu [15], and J. G. Smith Jr. et al. [16] could well disperse CNTs successfully in the polymer solution through the functionalized method. The conductivity decreased to 23 S/m as the loading of CNTs at 23 wt-% by Long et al. [17] using the surface functionalization.

Before surface-grafting, MWNTs were functionalized to induce carboxyl groups attaching on the surface of MWNTs by oxidation via acid mixture. [18] The disadvantages of acid-treated CNTs were defects produced from acid treatment might restrict electric conductivity and lower aspect ratios. Robert J. Chen et al. [19] performed a non-covalent functionalization, involved a bifunctional molecule, 1-pyrenebutanoic acid, succinimidyl ester, irreversibly adsorbed onto the inherently hydrophobic surfaces of SWNTs, to preserve electrical conductivity without breaking the sp^2 nanotube structure.

In the architecture of electrically percolated CNT network embedded in a polymer, the contacts between neighboring carbon nanotubes in fact control the conductive paths of the nanocomposite and the contact resistance between CNTs is mainly contributed by the polymer coated on them, which electron transferring on CNTs was much easier than in polymer. The contact resistance across two contacting CNTs in following four systems, polystyrene (PS)-MWNTs,

polybenzoxazole (PBO)-MWNTs, pyrene-MWNTs and the ideal system, can be determined from percolation fitting.

3-2 Experimental Section

Acid treatment of MWNTs

MWNTs synthesized via a chemical vapor deposition method (purchased from DESUN Nano Inc., Taiwan) had tube diameter of 10–30 nm and 5–15μm in length. The as-received MWNTs were first purified by the paper described. [20, 21] The purified MWNTs were then sunk in a mixed acid of concentric H_2SO_4 and HNO_3 (3:2 in volume) at 150 ^oC for respectively 0.5 h, 1 h, 1.5 h and 2 h, resulting in attachment of carboxyl groups (-COOH) on the surface of MWNTs and reducing the tube lengths of MWNTs.

Surface-grafting PS procedure

After acid treatment, there were carboxyl groups (-COOH) induced on MWNTs to form MWNT-COOH. Surface-grafting PS on MWNTs was carried out by the following steps after acid treatment. [21] At first, 40 mg MWNT-COOH reacted with sodium ethoxylate (EtONa) under sonication for 1 h to generate MWNT-COONa. Then, MWNT-COONa and 1 ml 4-vinylbenzyl chloride (VBC) were mixed under sonication for 2 h to form MWNT-$COOCH_2(C_6H_4)CHCH_2$ through eliminating sodium chloride (NaCl). Into a 25 ml flask equipped with a reflux condenser and a magnetic stir bar, MWNT-$COOCH_2(C_6H_4)CHCH_2$ made from above procedure were added with 3 ml styrene monomer and 5 mg 2,2'-azobis-isobutyronitrile (AIBN) as an initiator at 100°C for 3 h to grow PS chains grafting on MWNTs (PS-MWNT). Monodisperse PS (M_w/M_n = 1.3) of molecular weight M_w = 2000000 (Pressure Chemical Co., U.S.A.) was used as the polymeric matrix to blend with PS-MWNT forming PS-MWNTs/PS composites.

Surface-grafting PBO procedure

PBO grafted on MWNTs were synthesized by means of two-step polymerization. (Scheme 1) To a 25ml glass flask equipped with a nitrogen injection and mechanical stirrer was added 377.58 mg (1mmole) 2,2-bis(3amino-4-aminophenol)

hexafluoropropane (Bis-APAF), 162.89 mg (2mmole) anhydrous pyridine and 4 ml anhydrous 1-Methyl-2-pyrrolidone (NMP). After Bis-APAF was completely dissolved in NMP, 207.16 mg (1mmole) isophthaloyl chloride (IC) was added slowly to the solution into a bath of ice water for 8 h The precursor of PBO, poly(hydroxyamide) (PHA), precipitated in deionized water, and then reacted with MWNT-COCl made from the chlorination reaction of MWNT-COOH with thionyl chloride ($SOCl_2$) in NMP at 40°C for 24 h forming PHA-MWNTs. The PHA grafted on MWNTs could convert into PBO upon subsequent heating at 350 ^{o}C for 8 h, and then the PBO-MWNTs were blended with PI to prepare PBO-MWNTs/PI composites.

π-π stacking modification

1-pyrenebutyric acid (97%, purchased form Aldrich) and (2-chloroethyl) trimethylammonium were used for dispersing MWNTs in the composites. First, 1-pyrenebutyric acid reacted with EtONa in toluene by sonication at 40 ^{o}C for 1 h, and then (2-chloroethyl) trimethylammonium chloride was added to stir overnight at 60 ^{o}C. The excess 1-pyrenebutyric acid and (2-chloroethyl) trimethylammonium chloride precipitated in acetone and deionized water through centrifugation, and the solvent was removed by a rotary evaporator. The pyrene-MWNTs were blended with poly(amic acid) (PAA) and cured at 300 ^{o}C for 8 h to form the pyrene-MWNT/PI composite. (Scheme 2)

Characterizations

A field emission scanning electron microscope (FE-SEM, JEOL JSM-6500) was used to observe the MWNTs dispersion and percolated network structure of MWNTs/polymer nanocomposites. Thermal gravimetric analyses (TGA) were performed on Perkin-Elmer thermal analysis TG/DTA system under the argon atmosphere with a heating rate of 10 ^{o}C /min. The microstructures of the samples were examined under a transmission electron microscope (TEM) of JOEL JEM-2010 with acceleration voltage of 200 KeV. The resistivity was measured by four-probe dc measurement. Fourier transform infrared (FTIR) spectra of the samples were recorded between 4000 and 400 cm^{-1} on a Bomem DA8.3 infrared

spectrophotometer.

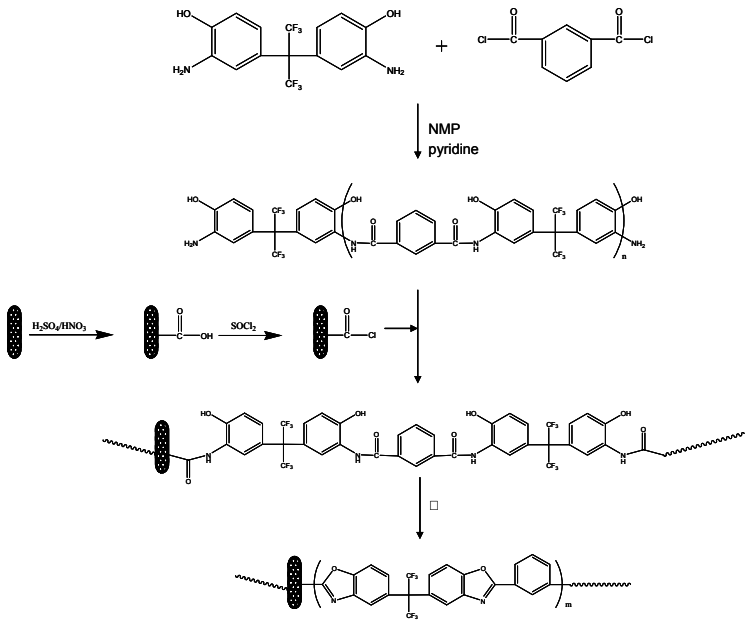

Scheme 1. The procedure of synthesis of PBO-MWNTs by following steps, including PHA formation, chlorination reaction of MWNT-COOH, surface-grafting PHA on MWNTs and curing.

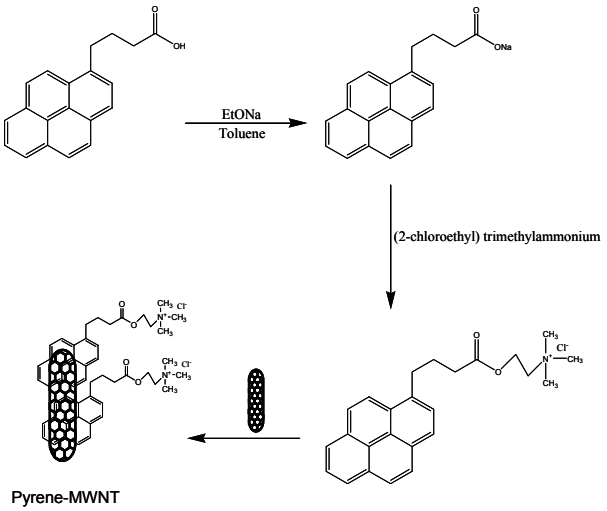

Scheme 2. The procedure of preparation of pyrene-MWNTs by π-π stacking modification which preserved high aspect ratios and unbroken sp^2 nanotube structure.

3-3 Results and discussions

The electrical resistivity of MWNTs grafted various amounts of carboxyl groups and aspect ratio lowering after acid treatment

The SEM observations of pristine and acid-treated MWNTs (MWNT-COOH) were respectively showed in Figure 1. The acid treatment was a step for decreasing aggregations obviously, and availed against surface grafting on the side-wall, but unfortunately, the conductivity of MWNTs was restricted by the carboxyl groups as defects for conducting. The films of MWNT-COOH were fabricated by spin coating and the resistivities were measured with different amounts of carboxyl groups attaching. The amounts of carboxyl groups on the surface of MWNTs were estimated by the method presented by H. Hu et al.. [22]

The resistivity of MWNTs have been reported between 10^{-4} and 10^{-5} Ω-cm [23]. The resistivity results of MWNT-COOH aimed to investigate the relationship between the concentration of carboxyl groups and electrical resistivity showed the resistivity increased quadratically with the number of surface carboxyl groups suggesting that carboxyl groups attack nanotubes on their intrinsic defects such as tips, pentagons and heptagons. (Figure 2)

Lengths of MWNTs decreased with reaction time of the acid treatment due to concentric acid might destroy nanotube structures and furthermore cut the nanotubes. (Figure 3) Aspect ratio of MWNTs, which reduced with lengths, led to the shorter conducting paths, though acid treatment was contributive to disperse MWNTs homogeneously to form percolating network structure in the nanocomposites.

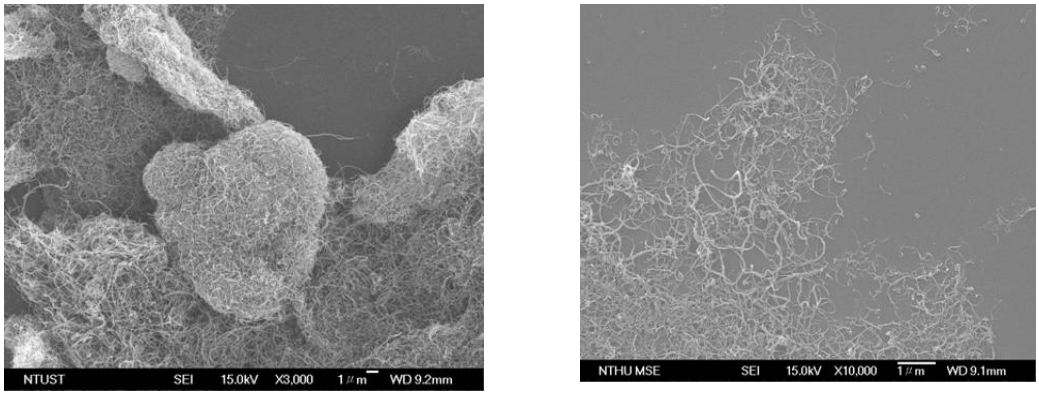

(a) **(b)**

Figure 1. The SEM micrographs of (a) pristine MWNTs showing the aggregates in evidence due to strong van der Waals attraction between them, (b) MWNT-COOH under acid treatment at 150 ^{o}C for 1 h showing well dispersion without the aggreagates because of carboxyl groups induced on the surface of MWNTs by concentric acid.

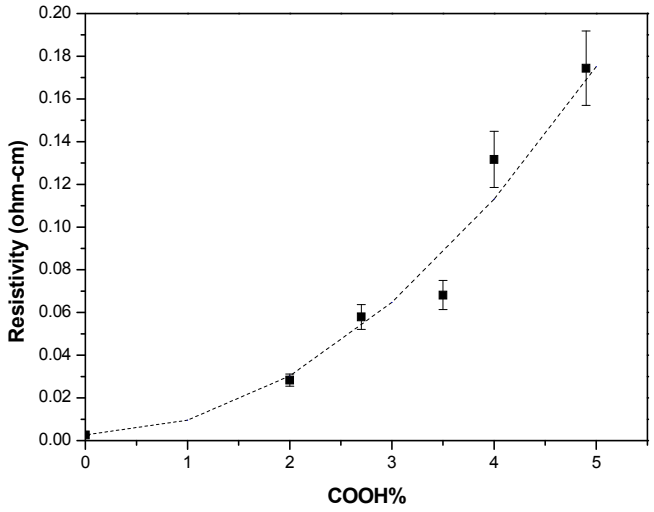

Figure 2. The electrical resistivity curve for acid-treated MWNTs (MWNT-COOH) indicated that carboxyl groups on the surface of MWNTs were restriction for conductivity of MWNTs.

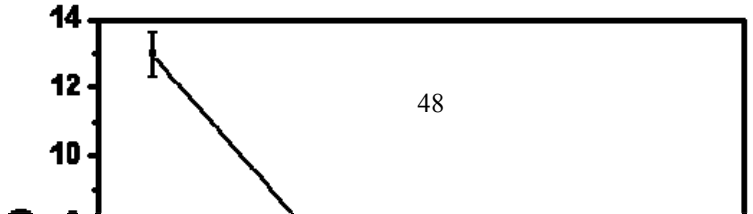

Figure 3. The lengths of MWNTs decreased with reaction time of acid treatment.

The PS-MWNTs/PS system

The percolating network structure was observed in the SEM micrographs which have been investigated in the papers we reported before. [20, 21] The resistivity results of PS-MWNTs/PS thin film indicated that the resistivity decreased sharply from 10^{15} Ω to 10^{7} Ω as the weight fraction of functionalized MWNTs becomes greater than 5%, while a weight fraction of the percolation threshold was less than 3%. (Figure 4) Resistivity of composites was often analyzed in terms of statistical percolation theory [24-28] , which the percolation equation is as follows:

$$\rho_c = \rho_o (f - f_c)^{-t} \qquad \text{for} \quad f > f_c$$

where ρ_c and ρ_o are respectively the resistivity of composite and conductive fillers, f_c is the percolation threshold fraction of fillers, and t is the critical exponent which strongly depends on the dimension of the lattice and the aspect ratio of the fillers with a range. The best fitting data from resistivity were 0.05 vol-% for f_c (the percolation threshold loading of fillers), 200000 Ω-cm for ρ_o (the resistivity of pure PS-MWNTs), and t was found around 2.7.

Although the resistivity has been improved greatly, the resistivity of the grafted nanotubes was greater than that without grafting about several orders because a

large contact resistance existed by the poor conductance (ρ_{PS} ~ 10^{14} – 10^{16} Ω-cm, compared to ρ_{CNT} ~ 10^{-3} – 10^{-6} Ω-cm) of the grafted PS between contact MWNTs in the nanocomposite.

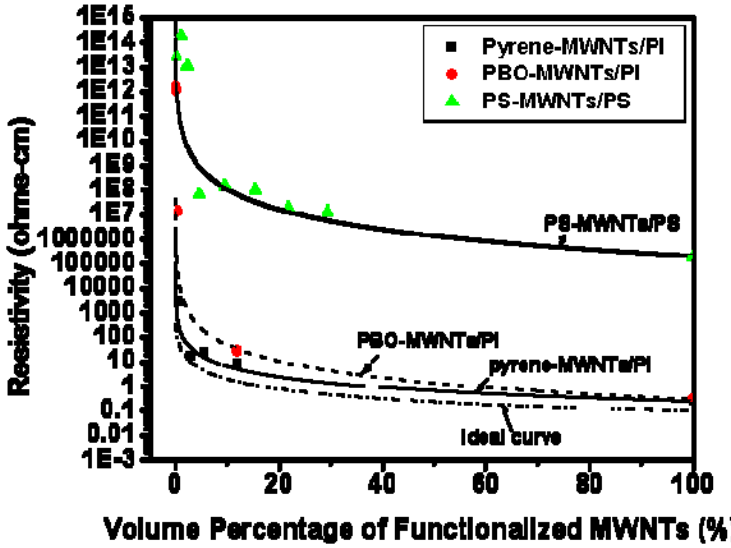

Figure 4. The resistivity curve of different polymer/MWNTs composites.

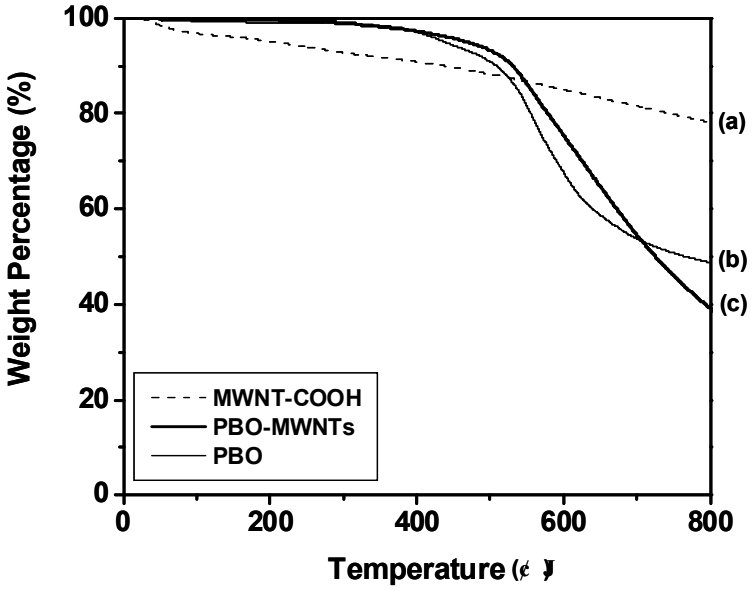

Figure 5. TGA analyses (a) MWNT-COOH, (b) PBO-MWNTs, and (c) pure PBO .

The PBO-MWNTs/PI system

TGA analyses were used to determine weight fraction of PBO grafting on MWNTs. (Figure 5) Sequentially, the residual weight percentage of MWNT-COOH, PBO-MWNTs, and pure PBO were respectively 78, 62, and 49 wt-% at 800 ^{o}C, indicating weight percentage of PBO grafting on MWNT was about 55 wt-%.

FT-IR spectra were used for characterizing the existence and transformation of PHA and PBO grafted on the MWNTs. (Figure 6) After grafting polymerization, an apparent peak was observed in the peak value of 1660 cm^{-1} indicating C=O groups from amide of PHA (Figure 6a) and the PHA grafted on MWNTs can be converted into PBO after heating at 350 ^{o}C for 8h, and the broaden peak of –OH (3100 – 3400 cm^{-1}) and the –NH peak (3300 – 3500 cm^{-1}) disappeared when PHA switched to PBO. (Figure 6b)

SEM observation of surface morphology of pure PI and PBO-MWNTs/PI composites indicated PBO-MWNTs dispersed homogeneously in the PI matrix and formed 3-dimentional percolating nanotube structure. (Figure 7) TEM images indicated PBO coated on the surface of MWNTs for PBO-MWNTs and therefore there were PBO existing between two contact nanotubes. (Figure 8) The resistivity of PBO-MWNTs/PI composites also could be fitted by the percolation theory as PS-MWNTs/PS system. The best fitting data were 0.499 vol-% for f_c, 0.3 Ω-cm for ρ_o (the resistivity of pure PBO-MWNTs), and t was found around 2.2. It suggested that the electrical resistivity of PBO-MWNTs was dramatically decreased by 6 orders of magnitude due to grafting polymer switching from PS to PBO for the purpose of decreasing the contact resistance. (ρ_{PBO} = 10^9 – 10^{10} Ω-cm; ρ_{PS} = 10^{14} – 10^{16} Ω-cm), and the resistivity greatly decreased at 2.6 vol-% loading of the functionalized MWNTs. (Figure 4)

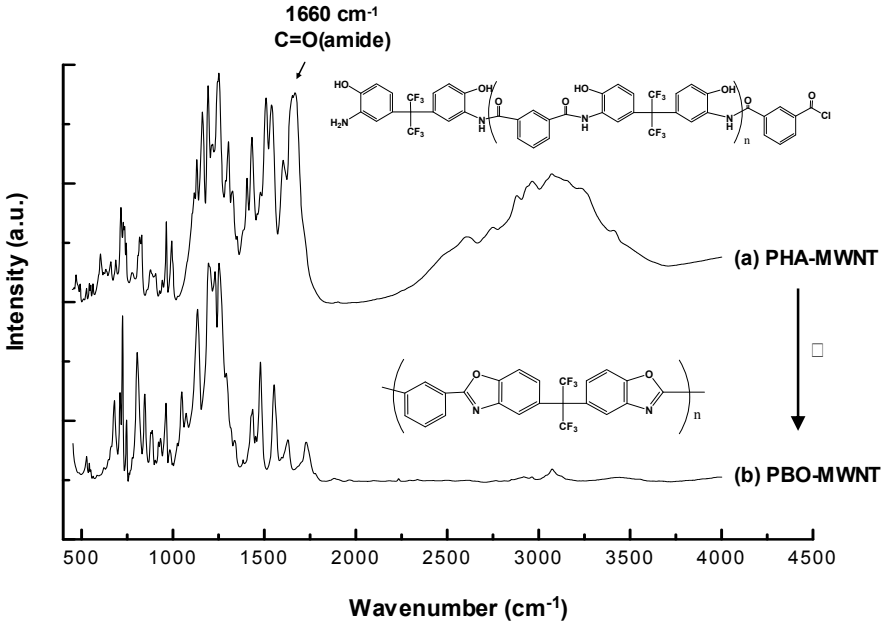

Figure 6. FT-IR spectra of (a) PHA-MWNTs (b) PBO-MWNTs.

The pyrene-MWNTs/PI system

The direct interaction of the nanotube surface and the pyrene moiety were obtained in NMP. SEM images showed not only a percolating network of MWNTs existing in pyrene-MWNTs/PI nanocomposites, but the longer lengths of MWNTs than the nanotubes through chemical functionalization. (Figure 9) The importance of π-π stacking of the pyrene moiety with the surface of MWNTs was suggested for solubilization of the nanotubes in solution. As mentioned before, the non-covalent modification could administer to maintain the great aspect ratios of MWNTs, not to destroy the sp^2 nanotube structure. The resistivity of pyrene-MWNTs/PI and PBO-MWNTs/PI would exhibit similar degree of decrease in resistivity due to better conductivity of PBO, although surface grafting PBO on MWNTs was a chemical functionalization that MWNTs had underwent an acid treatment. (Figure 4) The best fitting data from resistivity were 0.08 vol-% for f_c (the percolation threshold loading of fillers), 0.27 Ω-cm for ρ_o (the resistivity of pyrene-MWNTs), and t was found around 1.4.

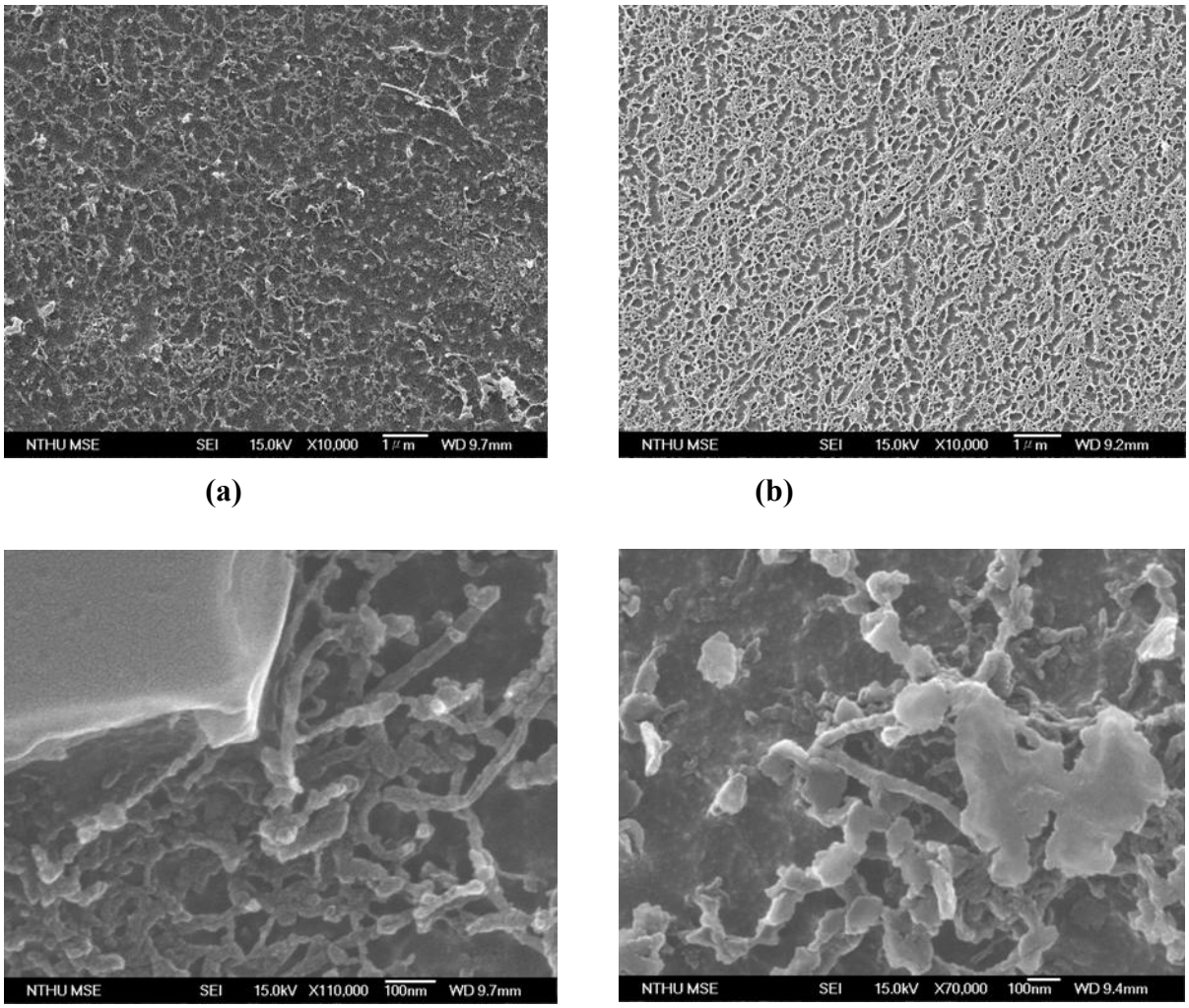

Figure 7. SEM images of surface morphology of plasma-etched films (a) pure PI, (b), (c), and (d) PBO-MWNTs/PI composite showing nanotube network and PBO were coated on MWNTs (PBO-MWNTs content = 2.6 wt-%).

Ideal MWNTs/polymer system

In order to analyze the effect of the polymer on nanotube sidewall [29], an ideal MWNTs/polymer composite was established to compare with three kinds of MWNTs/polymer systems mentioned above. The parameters for ideal model were 0.001 vol-% for f_c, 0.097 Ω-cm for ρ_o (the resistivity of pristine MWNTs), and 1.3 for t. Using the percolation equation, the curve for an ideal MWNTs/polymer composite, which defined as well dispersion, high aspect ratio of MWNTs, and the

fine conductivity property of polymer matrix, was created. As Figure 4 shown, pyrene-MWNTs/PI curve was much closed to the ideal curve because of more complete structure of MWNTs.

According to the fitting results, the f_c could demonstrate the dispersion of the MWNTs in the polymeric matrix, and t meant the dimension of nanotubes as the percolation threshold was reaching. The better dispersion was related to the lower t and f_c. Foygel et al. demonstrated that t equaled to 2 as the three dimension and would decrease to 1.1 – 1.4 as the aspect ratio increased [26], and our fitting results were consistent with their simulation works. For the more loading of functionalized MWNTs, the carriers could pass through more than one route, and thus the conducting paths of CNTs which are similar to the parallel circuit structures have been constructed.

Contact resistance

The contact resistance, R_c, between neighboring nanotubes along the percolated conducting paths, shown as Figure 10, was presented by S. D. Li et al.. [30] The equation is given by:

$$R = R_c + L \times 6000 k\Omega/\mu m$$

where L is the nanotube length meaning the length from one contact point to another one, and could be obtained from the result found by Foygel et al. [26] TGA analyses were used for measuring the weight percentage of polymer coated on the MWNTs and the molecular weight of polymer grafting on the surface of MWNTs was measured by GPC for calculating the polymer thickness on the surface of MWNTs. R_c was generated from the polymer thin layer which its thickness could be calculated by TGA and the molecular weight. Consequently, R_c could be calculated from R and $L \times \rho_o$. The contact resistance of PS-MWNTs, PBO-MWNTs and pyrene-MWNTs were respectively 2.12×10^{12}, 2.78×10^6 and 7.28×10^6 Ω. PS chains grafted on MWNTs possessed poor conducting properties resulting in the great contact resistance between neighboring PS-MWNTs and the conductivity of PI between the contact MWNTs in pyrene-MWNTs/PI nanocomposite was smaller than PBO in PBO-MWNTs/PI nanocomposite. As a result of the contact resistance, PBO coated on MWNTs was much useful to transport electron.

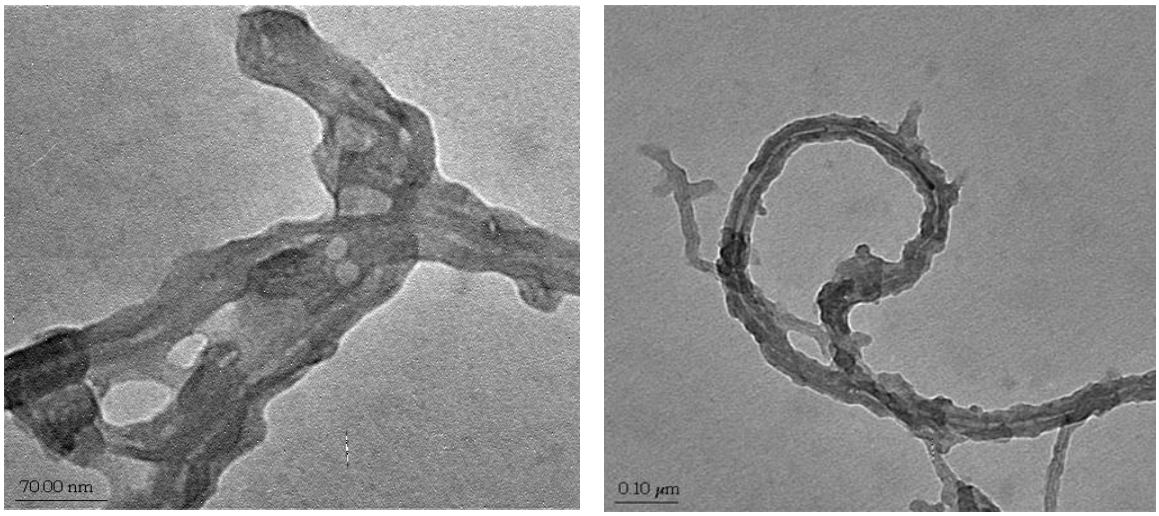

Figure 8. TEM images of PBO-MWNTs showing that PBO grafted on MWNTs was coated on the surface of them.

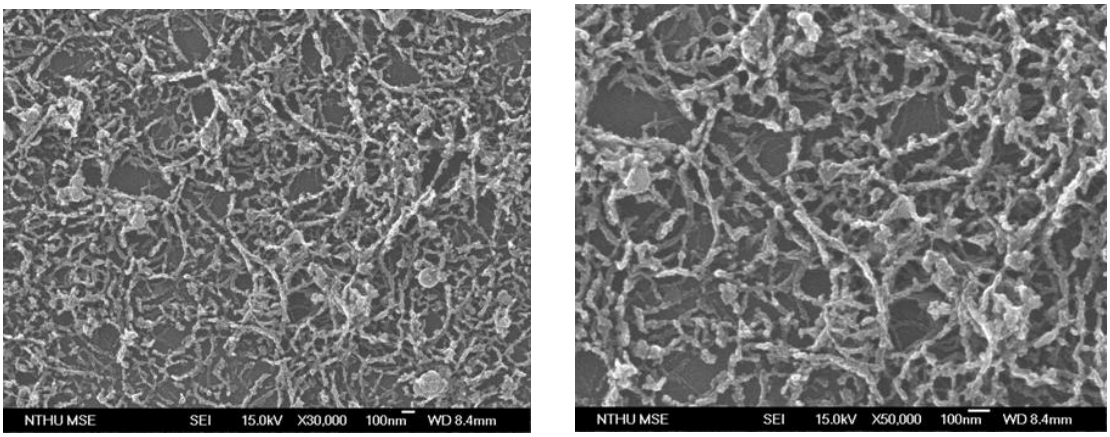

Figure 9. SEM images of pyrene-MWNTs/PI composite through oxygen plasma etching showing well dispersion of MWNTs and high aspect ratios. (pyrene-MWNTs content = 5 wt-%)

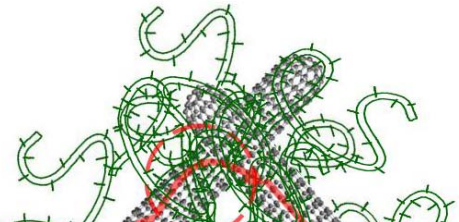

Figure 10. The modeling for the electron transmission through different nanotubes.

3-4 Conclusions

Degree of conductivity lowering depended on reaction time of acid treatment and increased with it due to the defects induced in the reflux of concentric acid in high temperature, and resistivity increased quadratically with the amounts of carboxyl groups. Well dispersion of the functionalized MWNTs via surface-grafting or π-π stacking modification in the polymeric matrix was revealed under SEM observations. The electrical properties of the three kinds nanocomposites were all improved for several orders of magnitudes after the percolation threshold, even chemical functionalization affected the conductivity of the MWNTs. As a result, resistivity test of the nanocomposites can demonstrate extremely high electric conductivity was much closed to the ideal theoretical prediction with proper selection of the grafted polymer. The molecular conformation of the grafted polymer and the intrinsic conductivity of the polymer strongly influence the final conductance of MWNTs/polymer composites, which PBO grafted on MWNTs was useful to decrease the contact resistance between neighboring MWNTs.

3-5 Reference

[1] S. Iijima, *Nature* **1991**, *354*, 56.

[2] X. W. Jiang, Y. Z. Bin, M. Matsuo, *Polymer* **2005**, *46*, 7418.

[3] Z. Ounaies, C. Park, K. E. Wise, E. J. Siochi, J. S. Harrison, *Compos Sci Technol* **2003**, *63*, 1637.

[4] H. Ago, M. S. P. Shaffer, D. S. Ginger, A. H. Windle, R. H. Friend, *Phys Rev B* **2000**, *61*, 2286.

[5] E. Bekyarova, M. E. Itkis, N. Cabrera, B. Zhao, A. P. Yu, J. B. Gao, R. C. Haddon, *J Am Chem Soc* **2005**, *127*, 5990.

[6] Z. M. Dang, C. W. Nan, D. Xie, Y. H. Zhang, S. C. Tjong, *Appl Phys Lett* **2004**, *85*, 97.

[7] N. Grossiord, J. Loos, O. Regev, C. E. Koning, *Chem Mater* **2006**, *18*, 1089.

[8] Y. J. Kim, T. S. Shin, H. D. Choi, J. H. Kwon, Y. C. Chung, H. G. Yoon, *Carbon* **2005**, *43*, 23.

[9] S. P. Li, Y. J. Qin, J. H. Shi, Z. X. Guo, L. Yongfang, D. B. Zhu, *Chem Mater* **2005**, *17*, 130.

[10] X. F. Lu, J. N. Zheng, D. M. Chao, J. Y. Chen, W. J. Zhang, Y. Wei, *J Appl Polym Sci* **2006**, *100*, 2356.

[11] T. McNally, P. Potschke, P. Halley, M. Murphy, D. Martin, S. E. J. Bell, G. P. Brennan, D. Bein, P. Lemoine, J. P. Quinn, *Polymer* **2005**, *46*, 8222.

[12] T. Ogasawara, Y. Ishida, T. Ishikawa, R. Yokota, *Compos Part a-Appl S* **2004**, *35*, 67.

[13] J. Sandler, M. S. P. Shaffer, T. Prasse, W. Bauhofer, K. Schulte, A. H. Windle, *Polymer* **1999**, *40*, 5967.

[14] Y. L. Yang, M. C. Gupta, K. L. Dudley, R. W. Lawrence, *Nanotechnology* **2004**, *15*, 1545.

[15] B. K. Zhu, S. H. Xie, Z. K. Xu, Y. Y. Xu, *Compos Sci Technol* **2006**, *66*, 548.

[16] J. G. Smith, J. W. Connell, D. M. Delozier, P. T. Lillehei, K. A. Watson, Y. Lin, B. Zhou, Y. P. Sun, *Polymer* **2004**, *45*, 825.

[17] Y. Z. Long, Z. J. Chen, X. T. Zhang, J. Zhang, Z. F. Liu, *J Phys D Appl Phys* **2004**, *37*, 1965.

[18] J. Zhang, H. L. Zou, Q. Qing, Y. L. Yang, Q. W. Li, Z. F. Liu, X. Y. Guo, Z. L. Du, *J Phys Chem B* **2003**, *107*, 3712.

[19] R. J. Chen, Y. G. Zhang, D. W. Wang, H. J. Dai, *J Am Chem Soc* **2001**, *123*, 3838.

[20] C. C. Hsiao, T. S. Lin, L. Y. Cheng, C. C. M. Ma, A. C. M. Yang, *Macromolecules* **2005**, *38*, 4811.

[21] T. S. Lin, L. Y. Cheng, C. C. Hsiao, A. C. M. Yang, *Mater Chem Phys* **2005**, *94*, 438.
[22] H. Hu, P. Bhowmik, B. Zhao, M. A. Hamon, M. E. Itkis, R. C. Haddon, *Chem Phys Lett* **2001**, *345*, 25.
[23] H. J. Dai, E. W. Wong, C. M. Lieber, *Science* **1996**, *272*, 523.
[24] I. Balberg, *Phys Rev Lett* **1987**, *59*, 1305.
[25] I. Balberg, N. Binenbaum, N. Wagner, *Phys Rev Lett* **1984**, *52*, 1465.
[26] M. Foygel, R. D. Morris, D. Anez, S. French, V. L. Sobolev, *Phys Rev B* **2005**, *71*.
[27] S. Kirkpatrick, *Rev. Mod. Phys.* **1973**, *45*, 574.
[28]E. J. Garboczi, K. A. Snyder, J. F. Douglas, M. F. Thorpe, *Phys Rev E* **1995**, *52*, 819.
[29] H. Park, J. J. Zhao, J. P. Lu, *Nano Lett* **2006**, *6*, 916.
[30] S. D. Li, Z. Yu, C. Rutherglen, P. J. Burke, *Nano Lett* **2004**, *4*, 2003.

Chapter 4

Synthesis of Carbon Nanotube Gels

Abstract

In this study, electric conductive properties of multi-walled carbon nanotubes (MWNTs)/polymer nanocomposite was investigated in the percolating network system after improving dispersal of MWNTs as conductive fillers in the polymeric matrix via surface-grafting polystyrene (PS) and polybenzoxazole (PBO), and modification by means of π-π stacking without breaking sp^2 nanotube structure. The amounts of carboxyl groups on MWNTs through acid treatment and resistivity of MWNTs with various amounts of carboxyl groups were quantitatively determined. Resistivity decreases with weight fraction of functionalized MWNTs and the results confirm the percolation behavior. Surface grafted nanotubes can substantially reduce the electrical conductivity if the grafted polymer is an electrical insulator. For 3~5 vol-% of functionalized MWNTs content in PS-MWNTs/PS composites which MWNTs was grafted to PS, MWNTs in the composites formed a percolating network and the value of electric resistivity decreased sharply by 7 orders of magnitude and furthermore decreased by a factor of 10^6 by switching the grafting polymer from PS to PBO. The pyrene-functionalized MWNTs were prepared by employing π-π stacking via sonication and were blended with polyimide (PI) as a matrix, and the resistivity results indicate the great improvement in the electronic property due to more complete nanotube structure. The resistivities of these different MWNTs/polymer composites based on percolation theory are best fit and furthermore the contact resistance across two contacting CNTs can be evaluated.

4-1Introduction

Since the landmark work by Iijima [1] in 1991, carbon nanotubes (CNTs), which possess remarkable thermal, electronic, mechanical [2-6] and geometrical properties, have attracted considerable attentions. They have been widely considered as an ideal candidate as reinforcing fillers for nanocomposites, mostly

in polymer matrices, owing to their extremely high Young's modulus, stiffness, flexibility, conductivity, and field emission properties.[5,7] However, due to the tendency of CNTs to aggregate [8-19] and the finite lengths of individual nanotubes, applications of CNTs had been severely limited. Homogeneous dispersion of CNTs or exfoliation of the aggregates was prerequisite to realization of the distinguished properties of individual CNTs in a nanocomposite.[20]

There have been two main methods for improving CNT dispersion, i.e., physical blending and chemical functionalization. For the former, sonication and stirring were used to force the dispersal of CNTs. [17,21] For examples, Qian et al. [21] had used a simple solution-evaporation method assisted by high energy sonication to prepare polystyrene (PS)/multi-walled carbon nanotubes (MWCNTs) composite films, in which MWCNTs were dispersed homogeneously in the PS matrix. Physical means also include addition of a surfactant or a compatibilizer that would break CNT aggregations and enhance matrix affinity.[22,23] For chemical functionalization, surface grafting with selected polymer chains, already commonly used, produces CNTs of modified surfaces that showed greatly enhanced compatibility to a polymeric matrix. In this, Holzinger et al. [24] functionalized single-walled carbon nanotubes (SWCNTs) and then crosslinked the SWCNTs by means of cycloaddition via nitrene. Separately, we had performed a method,[25,26] through free radical polymerization from anchored carboxyl groups on MWCNTs introduced by controlled acid treatments,[27] that had led to macroscopic uniform dispersion of MWCNTs in PS. In these MWCNT/PS nanocomposites, large shift of micro-deformation behavior and a dramatic increase in fracture toughness were observed.[26]

As a further step beyond surface grafting, a CNT gel, in which the CNTs are covalently bonded together through long connecting polymeric chains that effectively form a 3-dimensional crosslinked system featured with well-dispersed CNTs within-in, appears to be quite attractive. The crosslinked network of CNT gels provides opportunities for continuous paths of transferring electrons, phonons, or even mechanical stresses, provided that appropriate connecting polymer chains have been employed. For examples, conducting polymer chains bonded to CNTs provide direct conductive paths for transferring electrons. When linked with

biodegradable polymer chains, the CNT gels can be used as nanoporous tissue scaffolds that exhibit good mechanical strength supported by the CNTs. Also, the CNT gel will be demonstrating superior thermal stability and conductivity if rigid polymers such as poly(benzoxazole) (PBO) [28] is used. Furthermore, swollen CNT gels can be applied, after freeze-drying, for optoelectronics devices, biomedical applications, or heat sinks. In this study, poly(4-vinylbenzyl chloride) (PVBC) was selected as the connecting polymeric chains for demonstrating the synthesis feasibility.

4-2 Experimental Part

Functionalization of MWCNTs

MWCNTs synthesized via chemical vapor deposition (DESUN Nano Inc., Taiwan) were used, of which the average diameter was 10□30 nm and the length 5 □15μm, as revealed by electron microscopy. The as-received MWCNTs (1 g) first underwent the surface treatment of refluxing with 50 ml of concentrated sulfuric acid (98 wt %) and concentrated nitric acid (16 M) (v/v=3/2) at 150°C for 1 h to anchor carboxyl groups (□COOH) on the MWCNT surfaces. Graft polymerization of PVBC on the treated MWCNTs (MWCNT-COOH) was then carried out through steps as shown in Figure 1. In details, firstly the MWCNT-COOH (40 mg) reacted with sodium ethoxylate (EtONa) (230 mg) in toluene (10 ml) at 40°C under sonication for 1 h to generate MWCNT-COONa. It was followed by esterification of MWCNT-COONa via addition of 4-vinylbenzyl chloride monomer (VBC) (1 ml) into the solution under sonication for 2 h to generate MWCNT-COOR (R = $CH_2(C_6H_4)CHCH_2$). Then, in a 50 ml one-necked round-bottomed flask equipped with a reflux condenser and a magnetic stirring bar, the MWCNT-COOR reacted with VBC monomer (3 ml) and the initiator of 2,2'-azobis-isobutyronitrile (AIBN) (5 mg) at 100°C for 3 h to grow PVBC chains on MWCNTs (MWCNT-g-PVBC).

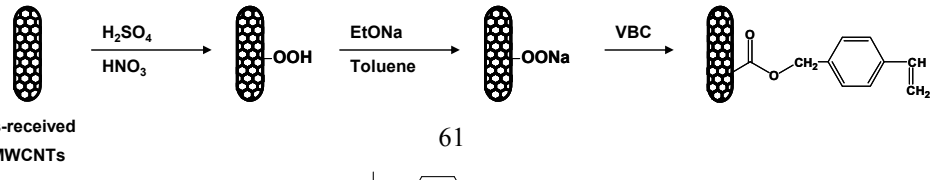

Figure 1. The process of functionalization of MWCNTs

Crosslinking Process

Free PVBC polymer was synthesized by heating the mixture of VBC monomer (3 ml) and AIBN (5 mg) without solvent in a 25 ml one-necked round-bottomed flask equipped with a reflux condenser and a magnetic stirring bar at 100 °C for 24 h. Crosslinking process was induced by the following steps as shown in Figure 2. MWCNT-g-PVBC (7.5 mg) was first added to PVBC (292.5 mg) in toluene (1 ml). After stirring for 10 minutes, a mixture of well-dispersed MWCNTs in PVBC matrix formed. Dissolving the mixture of MWCNTs/PVBC (MWCNTs content = 1 wt.-%) in toluene, a gel was observed at 9 h after addition of the crosslinker ethylenediamine (EDA) (0.025 ml) at room temperature. The MWCNT content was varied from 1 to 5 wt.% but for simplicity only the 1wt.% results were presented here.

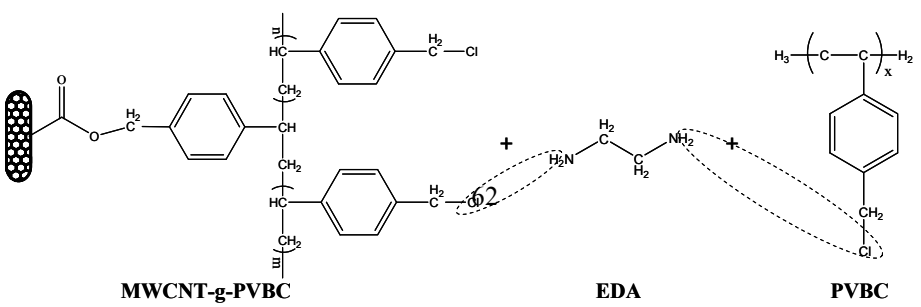

Figure 2. The crosslinking process of carbon nanotube gels (CNT gels).

Characterizations

Fourier-Transform Infrared spectroscopy (FT-IR) was used to monitor the occurrence of the crosslinking process with a infrared spectrophotometer (Bomem DA8.3) recording between 4000 and 400 cm^{-1}. Thermal gravimetric analyses (TGA) were performed under argon atmosphere with a heating rate of 10 °C/min (Perkin-Elmer thermal analysis TG/DTA system). A field emission scanning electron microscope (FE-SEM, JEOL JSM-6500) was used to observe the surface morphology of CNT gels. Measurements of molecular weight and polydispersity index (PDI) of the free PVBC polymer and grafted PVBC chains (after being cleaved from MWCNTs by KOH refluxing) were carried out by using gel permeation chromatography (GPC) analyses with PS standard calibrations.

4-3 Results and Discussion

The amount of linear polymer chains of PVBC grafted on MWCNTs was determined by TGA analyses (Figure 3). As a base line for the calculation, the TGA curve of the as-received MWCNTs was first determined, which showed a weight retention of 96% at 800 °C, with impurities and trapped water attributed to the 4% weight loss. The attachment of carboxyl groups during the acid treatment gave rise to an additional weight loss of 20% at 800 °C, as shown by the pyrolysis curve of

MWCNT-COOH. For the PVBC-grafted MWCNTs, the retention weight decreased sharply as temperature passed the temperature range between 200 and 400°C, and thereafter maintained a decreasing slope similar to that of the MWCNT-COOH pyrolysis curve. The difference between the weight losses of MWCNT-COOH and MWCNT-g-PVBC represents the weight fraction of PVBC grafted on MWCNT-g-PVBC, determined to be approximately 60%. The amount of PVBC grafted to the MWCNTs was controlled by varying the amount of carboxyl groups on the MWCNTs and the molecular weight of PVBC. As will be shown later, the PVBC chains grafted on MWCNTs were essential to good dispersion of MWCNTs in the PVBC matrix. For the sake of simplicity, data of one polymer fraction is presented here.

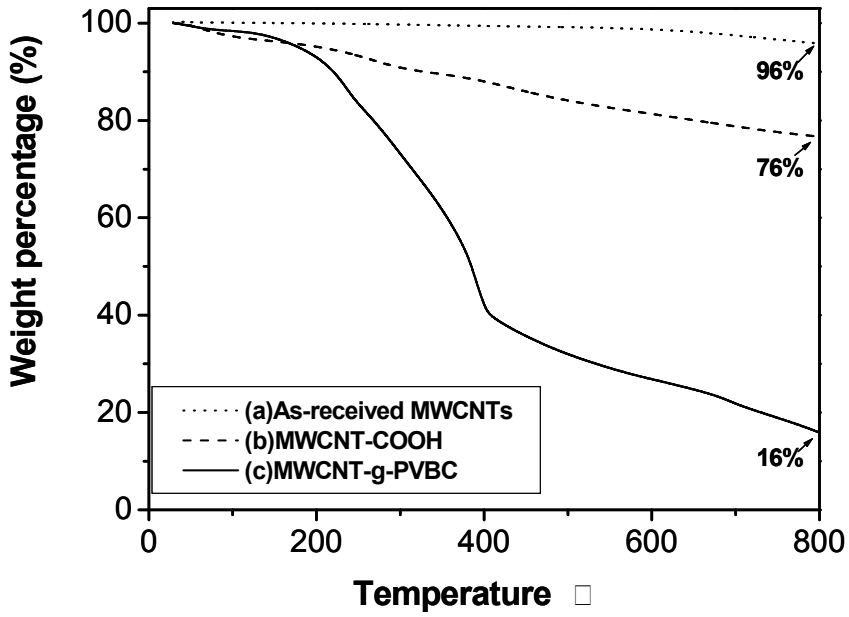

Figure 3. TGA analyses of (a) as-received MWCNTs, (b) MWCNT-COOH, and (c) MWCNT-g-PVBC.

Gelation was observed at about 9 h after the crosslinking process began at room temperature. Observations that the stirring bar no longer rotating (Figure 4a) and the emergence of a transparent gel insoluable in the solution served as a clear indication that the composite had crosslinked. The gel swelled by roughly a factor of 10 when immersed into a toluene bath for 3 days (Figures 4b), exhibiting excellent swelling property, which was resulted from the great length of polymer

chains between CNTs and can be controlled by the level of crosslinking density.

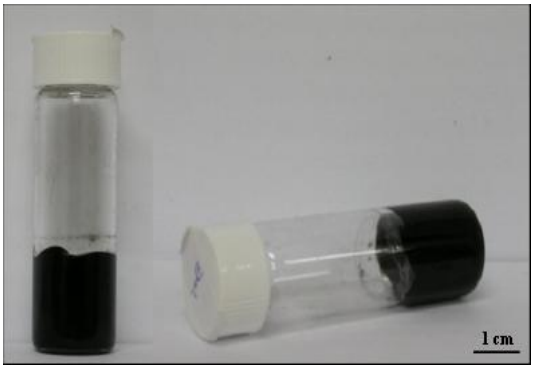

(a)

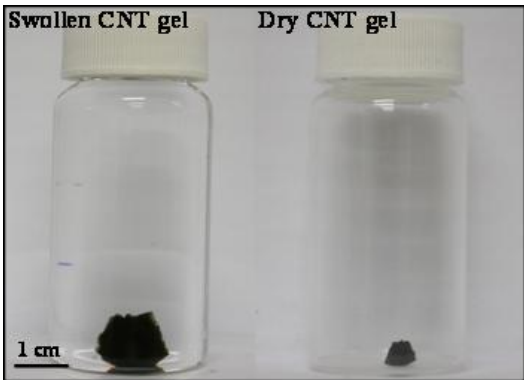

(b)

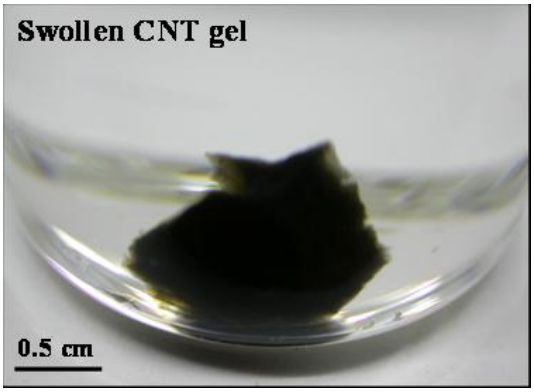

(c)

Figure 4. Photographs of CNT gels (MWCNTs content = 1 wt.%): (a) CNT gel without flowing, (b) swollen CNT gel and dry CNT gel (from left to right), and (c) swollen CNT gel.

FT-IR spectra (Figure 5) revealed the change from the primary amines to the secondary amines in the samples as a result of the crosslinking reaction. During the crosslinking procedure, hydrochloric acid (HCl) molecules were generated and eliminated from the reaction of □NH_2 groups of EDA and □CCl groups of PVBC, hence the primary amines transformed to the secondary amines. The primary amines, R-NH_2, show two N-H stretching bands in the range 3500-3200 cm^{-1}, whereas the secondary amines, R_2-NH, show only one stretching band in the same region.[29] The minor broad peak in the range 3600-3250 cm^{-1} is due to the

un-reacted □OH groups remaining on the MWCNTs.

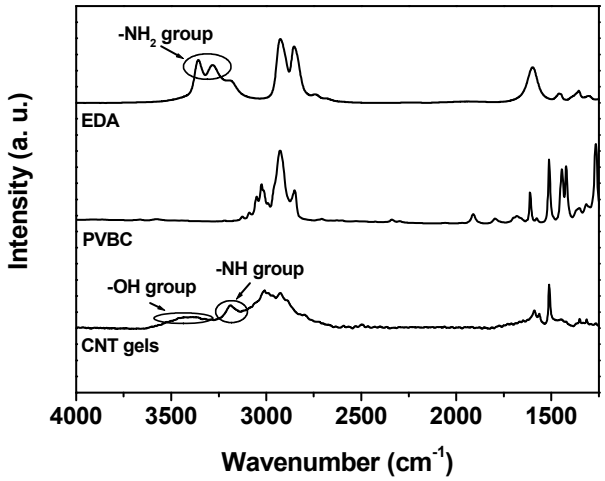

Figure 5. FT-IR spectra of EDA, PVBC, and CNT gels.

To determine the molecular weight of the grafted PVBC chains, the grafted macromolecules were cut from the nanotubes by refluxing MWCNT-PVBC in KOH (1M) for 2 days. GPC measurements were then made on the solutions with the MWCNTs filtered out. According to GPC analyses, the molecular weight (M_w) of the MWCNT-grafting PVBC and the free PVBC of the host matrix (M_w/M_n = 1.28) is respectively about 35200 and 104000 g/mole.

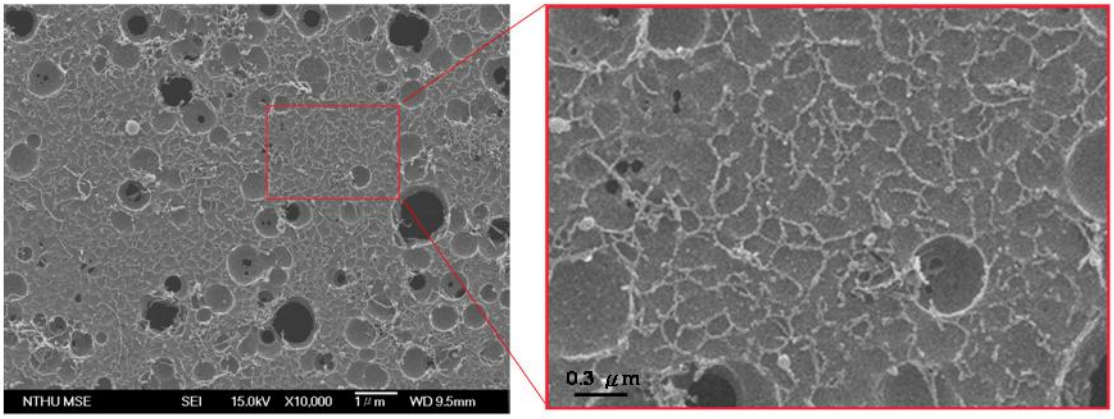

Figure 6. SEM micrograph of plasma-etched CNT gels showing the well-dispersed MWCNTs network.

Samples of different geometries can be cast before the step of crosslinking. For thin films, solutions of the MWCNTs-PVBC, the linear PVBC, and EDA in

toluene were used to cast films by spin coating. It was then followed by in-situ crosslinking. Such films were prepared and etched by mild oxygen plasma at 60 Watt for 30 minutes to reveal the MWCNTs distribution in the gel for SEM observations.[25,26] SEM micrographs of CNT gels (Figure 6) indicated that MWCNTs were dispersed in the gel homogeneously in global scales and had formed a percolated network. The cavities on the surfaces of both films are due to evaporation of trapped solvent in the relatively thick films.

The crosslinking density v_c (mole/cm^3) of the polymer was determined by the solvent swelling method [30] in which crosslinked polymer was immersed into a bath of toluene, a good solvent for PVBC, until the solvent sorption had saturated. The crosslink density v_c and hence the average molecular weight M_c of the strand between two crosslinking points ($\nu_c = \rho_2/M_c$) was calculated from the equilibrated polymer fraction X_{2m} in the fully soaked polymer by

$$M_c = \frac{-V_1\rho_2(X_{2m}^{1/3} - X_{2m}/2)}{\ln(1-X_{2m}) + X_{2m} + \chi X_{2m}^2}$$

where V_1 is the molar volume of the solvent, ρ_2 is the polymer mass density, and χ is the polymer-solvent interaction parameter. The χ parameter was taken from PS-toluene systems due to the similarity of chemical structures of PS and PVBC, which was approximately about 0.352 [31]. The mass density was determined directly from measurements of the sample weights and volumes. The equilibrated polymer fraction X_{2m} was obtained from the weight gain ($W_s - W_0$) using

$$X_{2m} = \frac{W_0}{V_{equil}\rho_2}$$

and

$$V_{equil} = \frac{W_0}{\rho_2} + \frac{W_s - W_0}{\rho_1},$$

where W_0 and W_s were the polymer weights before and after soaking, and ρ_1 the density of solvent. As obtained from the result of measurements and calculations, value of v_c and M_c were found to be respectively about 4.16×10^{-5} mole/cm^3 and

24900 g/mole. Chemical bonding between MWCNTs and PVBC matrix in the crosslinked system was re-confirmed because M_w of PVBC grafted on MWCNTs was greater than M_c. There were respectively 1.4 and 4.17 crosslinking points in average per PVBC chain grafted on MWCNTs and PVBC matrix.

The synthesis performed in this study provided a pathway to crosslink MWCNTs with polymeric chains to form CNT gels that also achieve good dispersion of MWCNTs. Substituting all or parts of the VBC, i.e., the chloride groups (□Cl), with other monomer would be a feasible alternative process to prepare other types of CNT gels. The amounts of crosslinking points can be controlled by the stoichiometry of EDA and the chemical structure of the linear chains. Clearly, the CNT gels will provide a new opportunity to novel nanocomposites that can be further tailored for numerous unique properties.

4-4 Conclusion

In this study, a technique of synthesizing CNT gels of percolated connectivity by connecting well-dispersed CNTs with long polymer chains is reported. Excellent swelling property of the CNT gels in good solvent baths provided clear evidence for the formation of the gel. Good dispersion of MWCNTs in the crosslinked system was revealed by SEM observations on the plasma-etched thin film of CNT gels. This new class of materials may provide important unique functions for emerging applications such as micro-heat sinks, bio-scaffolds, and photovoltaic devices.

4-5 References

[1] S. Iijima, *Nature* **1991**, *354*, 56.

[2] J. W. Mintmire, C. T. White, *Carbon* **1995**, *33*, 893.

[3] P. Poncharal, Z. L. Wang, D. Ugarte, W. A. de Heer, *Science* **1999**, *283*, 1513.

[4] R. S. Ruoff, D. C. Lorents, *Carbon* **1995**, *33*, 925.

[5] M. M. J. Treacy, T. W. Ebbesen, J. M. Gibson, *Nature* **1996**, *381*, 678.

[6] E. W. Wong, P. E. Sheehan, C. M. Lieber, *Science* **1997**, *277*, 1971.

[7] B. I. Yakobson, C. J. Brabec, J. Bernholc, *Phys Rev Lett* **1996**, *76*, 2511.

[8] H. Ago, M. S. P. Shaffer, D. S. Ginger, A. H. Windle, R. H. Friend, *Phys Rev B*

2000, *61*, 2286.

[9] E. Bekyarova, M. E. Itkis, N. Cabrera, B. Zhao, A. P. Yu, J. B. Gao, R. C. Haddon, *J Am Chem Soc* **2005**, *127*, 5990.

[10] Z. M. Dang, C. W. Nan, D. Xie, Y. H. Zhang, S. C. Tjong, *Appl Phys Lett* **2004**, *85*, 97.

[11] N. Grossiord, J. Loos, O. Regev, C. E. Koning, *Chem Mater* **2006**, *18*, 1089.

[12] Y. J. Kim, T. S. Shin, H. D. Choi, J. H. Kwon, Y. C. Chung, H. G. Yoon, *Carbon* **2005**, *43*, 23.

[13] S. P. Li, Y. J. Qin, J. H. Shi, Z. X. Guo, L. Yongfang, D. B. Zhu, *Chem Mater* **2005**, *17*, 130.

[14] X. F. Lu, J. N. Zheng, D. M. Chao, J. Y. Chen, W. J. Zhang, Y. Wei, *J Appl Polym Sci* **2006**, *100*, 2356.

[15] T. McNally, P. Potschke, P. Halley, M. Murphy, D. Martin, S. E. J. Bell, G. P. Brennan, D. Bein, P. Lemoine, J. P. Quinn, *Polymer* **2005**, *46*, 8222.

[16] T. Ogasawara, Y. Ishida, T. Ishikawa, R. Yokota, *Compos Part a-Appl S* **2004**, *35*, 67.

[17] J. Sandler, M. S. P. Shaffer, T. Prasse, W. Bauhofer, K. Schulte, A. H. Windle, *Polymer* **1999**, *40*, 5967.

[18] Y. L. Yang, M. C. Gupta, K. L. Dudley, R. W. Lawrence, *Nanotechnology* **2004**, *15*, 1545.

[19] B. K. Zhu, S. H. Xie, Z. K. Xu, Y. Y. Xu, *Compos Sci Technol* **2006**, *66*, 548.

[20] J. P. Salvetat, G. A. D. Briggs, J. M. Bonard, R. R. Bacsa, A. J. Kulik, T. Stockli, N. A. Burnham, L. Forro, *Phys Rev Lett* **1999**, *82*, 944.

[21] D. Qian, E. C. Dickey, R. Andrews, T. Rantell, *Appl Phys Lett* **2000**, *76*, 2868.

[22] Z. Jin, K. P. Pramoda, G. Xu, S. H. Goh, *Chem Phys Lett* **2001**, *337*, 43.

[23] Z. X. Jin, K. P. Pramoda, S. H. Goh, G. Q. Xu, *Mater Res Bull* **2002**, *37*, 271.

[24] M. Holzinger, J. Steinmetz, D. Samaille, M. Glerup, M. Paillet, P. Bernier, L. Ley, R. Graupner, *Carbon* **2004**, *42*, 941.

[25] T. S. Lin, L. Y. Cheng, C. C. Hsiao, A. C. M. Yang, *Mater Chem Phys* **2005**, *94*, 438.

[26] C. C. Hsiao, T. S. Lin, L. Y. Cheng, C. C. M. Ma, A. C. M. Yang, *Macromolecules* **2005**, *38*, 4811.

[27] J. Zhang, H. L. Zou, Q. Qing, Y. L. Yang, Q. W. Li, Z. F. Liu, X. Y. Guo, Z. L. Du, *J Phys Chem B* **2003**, *107*, 3712.

[28] C. W. Lin, J. Y. Lin, A. C.-M. Yang, C. C. M. Ma, "Surface grafting of carbon nanotubes with conjugated polybenzoxazole polymer", in *American Physical Society March Meeting*, Baltimore, Maryland, USA, 2006.

[29] D. L. Pavia, G. M. Lampman, G. S. Kriz, "*Introduction to Spectroscopy*", Brooks & Cole, 2001.

[30] U. W. Gedde, "*Polymer Physics*", Chapman & Hall, London, 1995.

[31] J. Brandrup, E. H. Immergat, "*Polymer Handbook*", John Wiley & Sons, 1989.